Received: 21 October 2019 | Accepted: 28 November 2019

DOI: 10.1111/gcb.15114

PRIMARY RESEARCH ARTICLE

Global Change Biology WILEY

Ensemble projections elucidate effects of uncertainty in terrestrial nitrogen limitation on future carbon uptake

Johannes Meyerholt[1,2†] | Kerstin Sickel[1] | Sönke Zaehle[1,3]

[1]Biogeochemical Integration Department, Max Planck Institute for Biogeochemistry, Jena, Germany

[2]International Max-Planck Research School Global Biogeochemical Cycles, Jena, Germany

[3]Michael Stifel Center Jena for Data-driven and Simulation Science, Jena, Germany

Correspondence
Sönke Zaehle, Biogeochemical Integration Department, Max Planck Institute for Biogeochemistry, Hans-Knöll-Str. 10, Jena 07745, Germany.
Email: szaehle@bgc-jena.mpg.de

Funding information
European Union, Grant/Award Number: 641816; European Research Council, Grant/Award Number: 647204

Abstract

The magnitude of the nitrogen (N) limitation of terrestrial carbon (C) storage over the 21st century is highly uncertain because of the complex interactions between the terrestrial C and N cycles. We use an ensemble approach to quantify and attribute process-level uncertainty in C-cycle projections by analysing a 30-member ensemble representing published alternative representations of key N cycle processes (stoichiometry, biological nitrogen fixation (BNF) and ecosystem N losses) within the framework of one terrestrial biosphere model. Despite large differences in the simulated present-day N cycle, primarily affecting simulated productivity north of 40°N, ensemble members generally conform with global C-cycle benchmarks for present-day conditions. Ensemble projections for two representative concentration pathways (RCP 2.6 and RCP 8.5) show that the increase in land C storage due to CO_2 fertilization is reduced by 24 ± 15% due to N constraints, whereas terrestrial C losses associated with climate change are attenuated by 19 ± 20%. As a result, N cycling reduces projected land C uptake for the years 2006–2099 by 19% (37% decrease to 3% increase) for RCP 2.6, and by 21% (40% decrease to 9% increase) for RCP 8.5. Most of the ensemble spread results from uncertainty in temperate and boreal forests, and is dominated by uncertainty in BNF (10% decrease to 50% increase for RCP 2.6, 5% decrease to 100% increase for RCP 8.5). However, choices about the flexibility of ecosystem C:N ratios and processes controlling ecosystem N losses regionally also play important roles. The findings of this study demonstrate clearly the need for an ensemble approach to quantify likely future terrestrial C–N cycle trajectories. Present-day C-cycle observations only weakly constrain the future ensemble spread, highlighting the need for better observational constraints on large-scale N cycling, and N cycle process responses to global change.

KEYWORDS

biogeochemical modelling, carbon–climate feedbacks, CO_2 fertilization, land surface models, model evaluation, terrestrial ecosystem modelling

†Deceased.

1 | INTRODUCTION

Over the last decades, the terrestrial biosphere has sequestered roughly a quarter of the CO_2 emitted by anthropogenic activities (Le Quéré et al., 2018). The future evolution of this carbon (C) uptake depends, among others, on the availability of nitrogen (N) to support this increase in terrestrial C (Hungate, Dukes, Shaw, Luo, & Field, 2003). Nitrogen is an essential nutrient for life, and therefore plant growth and soil microbial activity, but its availability is limited in most natural terrestrial ecosystems (Cleveland et al., 2013; Hyvönen et al., 2007; LeBauer & Treseder, 2008; Vitousek & Howarth, 1991). With the exception of two Earth System Models (ESMs), the Coupled Model Intercomparison Project Phase 5 (CMIP5; Jones et al., 2013) did not consider this N constraint, and thus likely overestimates the simulated future land C storage (Wieder, Cleveland, Smith, & Todd-Brown, 2015; Zaehle, Jones, Houlton, Lamarque, & Robertson, 2015).

Terrestrial biosphere models (TBMs) that estimate the future C-uptake potential of land vegetation increasingly consider the dynamics of the global N cycle and its linkage to the C cycle (Arora et al., 2019; Zaehle & Dalmonech, 2011). These models generally suggest that N constraints attenuate the land C response to global change (Sokolov et al., 2008; Thornton et al., 2009; Wårlind, Smith, Hickler, & Arneth, 2014; Zaehle, Friedlingstein, & Friend, 2010; Zhang, Wang, Matear, Pitman, & Dai, 2014). This is also the case in the new set of ESMs in the Coupled Model Intercomparison Project Phase 6 (CMIP6; Arora et al., 2019), where about half of the models include a N cycle representation. However, adequate ecosystem-scale characterization of terrestrial N cycle processes remains a challenge because of the complexity of N cycle processes, their spatial heterogeneity and the long-term cumulative effect of comparatively small fluxes such as biological nitrogen fixation (BNF) on ecosystem N availability (Thomas, Brookshire, & Gerber, 2015). As a consequence, the inclusion of N cycling in complex ESMs has been associated with considerable uncertainty, making it difficult to quantify the effect of N limitation in simulations of the biospheric C sink response to future global change (Zaehle & Dalmonech, 2011).

A better understanding of terrestrial N limitation in the Earth system requires the identification of the most important N-process mechanisms (Thomas et al., 2015). In the past, model comparisons that aimed to characterize the contribution of such N-related model uncertainties to model differences in future predictions were always confounded by alternative model structures not associated with the N cycle (Fleischer et al., 2019; Huntzinger et al., 2017; Medlyn et al., 2016; Thomas, Zaehle, Templer, & Goodale, 2013; Zaehle et al., 2014). Du et al. (2018) have recently highlighted the large difference in the simulated steady-state terrestrial N cycle by comparing selected components of the N cycle representation of three biosphere models within a common modelling environment. Here, we use an alternative approach that relies on the implementation and factorial combination of published strategies to represent N cycling in TBMs (Meyerholt & Zaehle, 2015, 2018; Meyerholt, Zaehle, & Smith, 2016; Table 1) into one common framework to provide a robust assessment of the likely range of future terrestrial C storage and attribution to underlying model assumptions.

We focus on the representation of processes that affect the long-term trajectories of the coupled land C and N cycles in response to changing atmospheric CO_2, climate and N deposition: processes that affect the ratio of C to N storage in the land biosphere, as well as the balance of ecosystem N in- and outputs (Gruber & Galloway, 2008; Hungate et al., 2003; Walker et al., 2015; Zaehle et al., 2014). Alternative assumptions about the dependence of BNF and N loss on plant N demand can lead to diverging responses of the terrestrial N balance to global changes, and therefore change the amount of N available to store C (Du et al., 2018; Meyerholt & Zaehle, 2018; Meyerholt et al., 2016; Wieder, Cleveland, Lawrence, & Bonan, 2015). Alternative assumptions about the flexibility of the plant and soil organic matter (SOM) C:N ratios affect the response of tissue-specific process rates (such as photosynthesis and respiration), the relative competitive strength of plants and SOM for N, and finally the amount of C that can be stored given a specific N amount (Meyerholt & Zaehle, 2015; Thomas et al., 2013).

We selected two C:N stoichiometry, five BNF and three N-loss algorithms, and used these to generate an ensemble of 30 factorial combinations of these algorithms within the O-CN C–N cycle model (Zaehle, Ciais, Friend, & Prieur, 2011; Zaehle & Friend, 2010, see Section 2). Here, we first analyse the C–N cycle ensemble with respect to its ability to simulate the global contemporary C and N cycle commensurate with observations. We then analyse the trajectories resulting from historical (1850–2005) and projected (2006–2099) changes of atmospheric CO_2, climate, and N deposition for two global change scenarios, specifically the representative concentration pathway (RCP) 2.6 (with an average global land air temperature (GLAT, but without Antarctica) increase of 2.4°C between 1850 and 2099) and 8.5 (GLAT increase of 8.0°C; Dufresne et al., 2013; Hempel, Frieler, Warszawski, Schewe, & Piontek, 2013; Meinshausen et al., 2011), and compare these to the C-only reference version of O-CN. We attribute model uncertainty to underlying process formulations and investigate to what extend a range of contemporary C-cycle benchmarks constrain the model spread. Based on this analysis, we estimate the anthropogenic emissions compatible with each RCP scenario, given the RCP-specific atmospheric CO_2 trajectory, simulated oceanic uptake (Dufresne et al., 2013), as well as the projected land C uptake considering N constraints.

2 | METHODS

2.1 | Model description

Model simulations were performed with the O-CN model (Zaehle et al., 2011; Zaehle & Friend, 2010), an extension of the ORCHIDEE model (Krinner et al., 2005), the land surface component of the Institute Pierre Simon Laplace (IPSL) climate model (Dufresne et al., 2013). O-CN describes a fully prognostic N cycle that accounts for ecosystem N input from atmospheric deposition and biological fixation, and N losses due to leaching of dissolved organic and

TABLE 1 Overview on the alternative nitrogen cycle algorithms employed in this study to represent carbon:nitrogen ratio (C:N) flexibility, biological nitrogen fixation (BNF) and ecosystem-level nitrogen losses. All algorithms, including their parameterizations are described in full in Meyerholt and Zaehle (2015; M1; C:N flexibility), Meyerholt et al. (2016; M2; BNF) and Meyerholt and Zaehle (2018; M3; nitrogen losses)

Model	Description	Reference	Documentation
C:N flexibility, see Section 2.1.1			
R1	PFT- and tissue-specific, time-invariant C:N in organic plant and soil pools	Sokolov et al. (2008), Thornton et al. (2009)	FIX in M1
R2	C:N in organic plant and soil pools flexible within prescribed, PFT-specific bounds	Zaehle and Friend (2010)	FLX in M1
Biological nitrogen fixation (BNF), see Section 2.1.2			
F1	Linear relationship with time-invariant climatology of actual evapotranspiration, set to zero above an soil inorganic N pool of 2 g N/m^2	Cleveland et al. (1999), Zaehle, Friedlingstein, et al. (2010)	FOR in M2
F2	Monotonically increasing, saturating function of the simulated time-variant annual net primary production	Cleveland et al. (1999), Goll et al. (2012), Thornton et al. (2009)	NPP in M2
F3	Linear relationship with the simulated time-variant annual actual evapotranspiration	Cleveland et al. (1999), Wårlind et al. (2014), Yang, Wittig, Jain, and Post (2009)	AET in M2
F4	Function of simulated plant N limitation and light limitation outside the tropics	Gerber et al. (2010)	NDS in M2
F5	Function of an optimality criterion based on the C cost of investment into root N uptake and the C cost of BNF	Rastetter et al. (2001)	OPT in M2
Ecosystem nitrogen losses, see Section 2.1.3			
L1	Explicit representation of the main gaseous and leaching N-loss pathways, depending each on the soil inorganic N pool size, temperature, moisture and water leaching	Li, Aber, Stange, Butterbach-Bahl, and Papen (2000), Xu-Ri and Prentice (2008), Zaehle et al. (2011)	NL1 in M3
L2	Fixed fraction of gaseous loss and leaching, based on the N mineralization flux and the soil inorganic N-pool size respectively	Wang et al. (2010)	NL2 in M3
L3	Sequential treatment of loss pathways of (a) net N mineralization-dependent denitrification; (b) volatilization and denitrification depending on the size of the mineral N pool; (c) leaching based on the mineral N pool	Thornton and Rosenbloom (2005), Thornton et al. (2009)	NL3 in M3

Note: Abbreviation: PFT, plant functional type.

inorganic N, as well as gaseous losses associated with volatilization, nitrification and denitrification. Once soil mineral N is taken up by plants, it cycles as organic N between different plant, litter and SOM pools, where its tissue-specific concentration affects among others plant photosynthesis and respiration, plant allocation to fine roots and vegetation growth. Soil mineral N availability also affects litter and SOM decomposition rates, as well as the rate of net N mineralization, which depends further on the difference in C:N stoichiometry of decomposing litter and SOM pools. Overall, the O-CN model has shown good performance against a range of global biosphere benchmarks (Le Quéré et al., 2018; Zaehle, Friend, et al., 2010, 2011).

To isolate the effect of N-cycle parameterization from other model structural assumptions of O-CN, we generated a C-only version of O-CN. This version assumes for each plant tissue-type or soil biogeochemical pool, vegetation-type specific, time-invariant N concentrations constrained by observed estimates (Kattge et al., 2011). In this model version, N is added to the plant labile N pool (soil mineral NH_4 pool) whenever limiting N availability would reduce plant growth (SOM decomposition). As a result, this model version responds to changes in atmospheric CO_2, temperature, precipitation and so on as the model without a full N cycle would. In particular, the response of terrestrial C gain to CO_2 is driven by the biochemical response embedded in the leaf-photosynthesis model (Kull & Kruijt, 1998), and only modulated due to the scaling from leaf to canopy, and the response of vegetation dynamics and turnover to changes in production (Zaehle & Friend, 2010). In a similar manner, other ecosystem processes, such as autotrophic and heterotrophic respiration respond to temperature and soil moisture, and are unaffected by N availability (Zaehle & Friend, 2010).

For the purpose of this study, the N cycle representation in O-CN was expanded to include alternative algorithms to represent the key N mechanisms of C:N ratio flexibility, BNF and N loss (Table 1; Sections 2.1.1–2.1.3). Each of the added algorithms was previously published and applied in N-enabled land C cycle models. The details of the equations, parameters and the implementation into the O-CN code are described by Meyerholt and Zaehle (2015; C:N flexibility), Meyerholt et al. (2016; BNF) and Meyerholt and Zaehle (2018; N losses). We combined these algorithms in a factorial manner to generate an ensemble of 30 C–N models (O-CN revision 295, see Meyerholt, Sickel, & Zaehle, 2019).

2.1.1 | Carbon:nitrogen ratios

Carbon:nitrogen ratios influence, for instance, leaf-specific photosynthetic efficiency through its dependence on foliar N content (Field & Mooney, 1986). They also affect the net N mineralization rate through its dependence on the difference between the C:N ratios of plant litter and SOM (e.g. Manzoni, Trofymow, Jackson, & Porporato, 2010). Finally, they affect the overall amount of N required for C storage (Hungate et al., 2003). Some models represent C:N ratios as time-invariant, tissue type-dependent constants, assuming that the observed difference of, for example, needle-leaved and broad-leaved foliage C:N ratio result from a tissue type-specific stoichiometric homeostasis of leaf growth and N supply (e.g. Sokolov et al., 2008; Thornton et al., 2009; C:N algorithm R1). However, ample experimental evidence suggests that foliar (and litter) C:N ratios decline under elevated CO_2, and increase with N fertilization (e.g. Ainsworth & Long, 2005; Magill et al., 2004; McNulty, Boggs, Aber, Rustad, & Magill, 2005). Although the exact mechanistic cause of these changes is uncertain, this has been represented empirically in a number of models (e.g. Wårlind et al., 2014; Zaehle, Friedlingstein, et al., 2010 C:N algorithm R2). The implications of flexible stoichiometry with increased N availability are on the one hand increased biochemical rates (photosynthesis, respiration, gross N mineralization and immobilization), and on the other hand decreased the ability to sequester C per unit plant or soil N.

2.1.2 | Biological nitrogen fixation

Biological nitrogen fixation through asymbiotic or symbiotic pathways is the most important form of N input in many natural ecosystems (Vitousek et al., 2002). Reflecting the lack of consensus about the mechanisms that control ecosystem-level BNF, there is a large range of published approaches ranging from a global, time-invariant map of BNF to process-oriented formulations that allow BNF to adjust to ecosystem N requirements. This choice does not only affect the geographic patterns of BNF, but also the response to ecosystem productivity, and therefore both the N capital of ecosystems in equilibrium and their response to global change. The simplest strategy, BNF algorithm F1, assumes that the large-scale pattern of BNF corresponds to patterns in long-term average climate conditions (Cleveland et al., 1999), but does not respond to environmental change at timescales considered in land surface models (as used e.g. in Zaehle, Friend, et al., 2010). BNF algorithm F2 relates BNF to net primary productivity as a saturating function (e.g. Thornton, Lamarque, Rosenbloom, & Mahowald, 2007), which, while derived from the study of Cleveland et al. (1999) has limited support from the data presented in that paper. BNF algorithm F3 (e.g. Goll et al., 2012; Smith et al., 2014), based on correlating BNF with simulated evapotranspiration (as in Cleveland et al., 1999), suggests that BNF increases with foliar coverage and productivity, but is reduced by water limitation or increasing atmospheric CO_2. In contrast to these phenomenological strategies, BNF algorithm F4 formulates BNF as a time-lagged response to vegetation N demand (or deficit to sustain growth), which furthermore considers a light limitation factor for non-tropical plants, reducing BNF in closed-canopy ecosystems (Gerber, Hedin, Oppenheimer, Pacala, & Shevliakova, 2010). BNF algorithm F5 is based on the principle of optimality of resource investment into nutrient acquisition, where BNF is regulated by the relative C cost of N uptake through BNF or root uptake, indirectly responding to plant N demand and supply (Meyerholt et al., 2016; Rastetter et al., 2001).

2.1.3 | Ecosystem nitrogen losses

Ecosystem nitrogen losses occur due to leaching of inorganic N or gaseous losses during volatilization, nitrification and denitrification (Gruber & Galloway, 2008). Some models simulate these processes explicitly (e.g. Xu-Ri & Prentice, 2008; Zaehle, Friend, et al., 2010, represented by loss algorithm L1). These models predict that plant N demand and net mineralization control N losses indirectly via changes in soil inorganic N concentrations. Thereby plants can affect the openness of the terrestrial N cycle, that is, the ratio of N loss to internal N turnover, in these models, which can increase plant available N in periods of N shortage through reduced N losses. A different strategy that requires fewer assumptions about uncertain subgrid soil processes (e.g. Wang, Law, & Pak, 2010; loss algorithm L2) is to hypothesize that the majority of N loss is directly related to soil N turnover, that is gaseous losses are calculated as a fixed fraction of the mineralization flux. In these models, plant N demand has limited control on N-cycle openness and therefore plant N availability. An intermediate strategy (Thornton et al., 2007), described by loss algorithm L3, applies a hierarchical structure, removing a fixed fraction of excess N left by soil immobilization, plant uptake and turnover-based denitrification losses to represent volatilization of reactive N species, further denitrification and leaching loss.

2.2 | Simulation setup

All model versions (30 C–N ensemble members and the one C-only version) were applied to run identical global simulation runs on a 2° by 2° spatial grid. The model C and N pools were spun up to equilibrium for conditions taken as representative for pre-industrial conditions, using 1850 N deposition rates (Lamarque et al., 2011), 1850 ambient CO_2 concentrations (Meinshausen et al., 2011) and randomly chosen climate forcing from the period 1901–1930. The climate data were taken from the CMIP5 projection of the IPSL general circulation model IPSL-CM5A-LR (Dufresne et al., 2013), bias-corrected according to the Inter-Sectoral Impact Model Intercomparison Project (Hempel et al., 2013). Land cover and mineral N input from artificial fertilizers were kept constant at year 2000, values taken from Hurtt et al. (2006) and Zaehle et al. (2011)

respectively. From 1850, we performed a number of simulations for the 1850–2099 period that varied in the applied transient forcing of atmospheric CO_2 (Meinshausen et al., 2011), N deposition (Lamarque et al., 2011) and climate (see also Figure S2a–c). Since the climate data were only available from 1901, for the period 1850–1900 climate of the years were randomly chosen as during the spin-up period (see Table 2).

2.3 | Model analyses

2.3.1 | Ensemble evaluation

We evaluated the simulated terrestrial productivity from the s3 experiment against two alternative estimates: a direct comparison against independent data-driven estimates based on the upscaling of site-based eddy-covariance measurements (Jung et al., 2011). As an alternative metric, we evaluated the long-term mean (1982–2011) polewards increase in the seasonal cycle amplitude of atmospheric CO_2. Although this increase reflects the balance of terrestrial productivity and respiration, it is strongly correlated with the large-scale latitudinal distribution of terrestrial productivity (Dalmonech & Zaehle, 2013; Heimann et al., 1998). As a simplified metric, we diagnosed the polewards increase in the seasonal cycle by regressing the detrended seasonal amplitude against the sine of latitude at the 13 long-term monitoring stations (Ω_{lat}, ppm/sin(lat)).

For comparison to atmospheric CO_2 measurements, the simulated monthly net land–atmosphere CO_2 fluxes for the years 1982 to 2011 from our 30 + 1 model versions were transported to 13 long-term atmospheric monitoring stations (Dalmonech & Zaehle, 2013; see Table S3 for the list of stations used) using the Jacobian representation of the TM3 atmospheric transport model, version 3.7.22 (Kaminski, Heimann, & Giering, 1999; Rödenbeck, Houweling, Gloor, & Heimann, 2003), with interannually varying wind fields (Kalnay et al., 1996, updated), together with estimates of the net ocean–atmosphere C flux (Jacobson, Mikaloff Fletcher, Gruber, Sarmiento, & Gloor, 2007; Mikaloff Fletcher et al., 2006; 2007), as well as estimated global fossil fuel emission fluxes (Boden, Marland, & Andres, 2013). We further evaluated the sensitivity of the atmospheric CO_2 growth rate to interannual climate variability (γ_{IAV}, ppm/K) by correlating the observed or simulated interannual CO_2 growth rate anomaly at the Mauna Loa station with interannual variations of the global land temperature. The temperature anomalies were derived from CRU-NCEP (Viovy, 2016) for the observed CO_2 record, and from the model forcing (bias-corrected IPSL-CM5A-LR; Dufresne et al., 2013; Hempel et al., 2013) for the simulations. Note that in the simulations, the atmospheric growth rate of CO_2 seen by the land models was derived from Meinshausen et al. (2011).

TABLE 2 Overview of the simulations performed

Simulation	CO_2	Climate	N deposition	Scenario
s0	–	–	–	n.a.
s1	X	–	–	RCP 8.5
s2	X	X	–	RCP 8.5
s3	X	X	X	RCP 8.5
s4	X	X	X	RCP 2.6

Note: X, transient forcing from 1850 to 2099; –, 1850 conditions for CO_2 and N deposition, or randomly chosen years of the climate forcing from year 1901 to 1930. s3 and s4 are identical until the year 2005.
Abbreviation: RCP, representative concentration pathway.

2.3.2 | Attribution of model spread to a particular algorithm

In order to characterize the effect of a particular model algorithm on the ensemble mean, we grouped ensemble members according to the algorithm used, for example model group R1 includes all ensemble members that employ the C:N algorithm R1. We then calculated the mean for this group ($\overline{M}_{group}$) and compared it to the mean of the entire ensemble ($\overline{M}_{ensemble}$). For comparability across different model outputs and regions, we calculated a normalized *z*-score as

$$z_{group} = \frac{\overline{M}_{group} - \overline{M}_{ensemble}}{SD_{ensemble}}, \quad (1)$$

where $SD_{ensemble}$ is the standard deviation of the entire ensemble. Note that the number of ensemble members (n) for the calculation of $\overline{M}_{group}$ differs across the process groups of C:N (n = 15), BNF (n = 6) and N loss algorithms (n = 10; see Table 1).

2.3.3 | Carbon-cycle sensitivities

For a better understanding of the N-cycling effect on projected land C storage (vegetation, litter and soil C) in the year 2099, we decomposed the change in land C into C-cycle sensitivities to changes in atmospheric CO_2 (β_L, Pg C/ppm) and climate change (γ_L, Pg C/K), as in Arora et al. (2013). Because our simulations consider transient changes in N deposition, an additional term to describe the carbon–nitrogen sensitivity (η_L, Pg C/Pg N), that is the change in land C in response to the cumulated amount of atmospheric N deposition was added to the framework.

$$\Delta C_L = \beta_L * (C_{A,2099} - C_{A,1850}) + \gamma_L * (\overline{T}_{2070-2099} - \overline{T}_{1850-1879}) + \eta_L * \sum_{i=1850}^{2099} (N_i - N_{1850}), \quad (2)$$

where ΔC_L is the simulated change in land C storage, C_A is atmospheric CO_2 (ppm), $\overline{T}$ is the global 30-year mean land air temperature (excluding Antarctica) and $\sum N$ is the cumulative N deposition on land, all between 1850 and 2099. These C-cycle sensitivities were derived from the factorial simulations s0–s3 as follows: The C–concentration sensitivity ($\beta_L = \Delta C_L/\Delta C_A$) was derived from the s1 to s0 difference in land C storage in the year 2099 and solely reflects the effects of atmospheric

CO_2. The C–N sensitivity ($\eta_L = \Delta C_L / \sum N$) was derived from the s2 to s1 difference in land C storage in the year 2099, and therefore accounts for potential synergistic interactions between the C-concentration and C–N sensitivities. The C–climate sensitivity ($\gamma_L = \Delta C_L / \Delta \overline{T}$) was derived as the difference between s3 and s2 land C storage in 2099 and therefore accounts for potential synergistic interactions between the C-concentration, C–N and C–climate sensitivities. The comparison of these sensitivities across studies needs to consider that these properties are known to be scenario dependent (Arora et al., 2013).

Estimates of the C-cycle response to C and N perturbations at global scale are scarce. In an attempt to provide an indication of plausibility of the simulations, we evaluate the ensemble by comparison of meta-analyses on plant growth responses of elevated CO_2 (Baig, Medlyn, Mercado, & Zaehle, 2015) and N addition experiments (Schulte-Uebbing & de Vries, 2018).

2.3.4 | Implied RCP-compatible emissions

In order to diagnose the N-related imprint on the anthropogenic C emissions compatible with the atmospheric CO_2 concentration pathways for the RCP2.6 and RCP8.5 scenarios ('RCP-compatible emissions' hereafter; Meinshausen et al., 2011; Zaehle et al., 2015), we followed a previously described approach (Jones et al., 2013): compatible emissions (E_i^{rcp}) for the 2006–2099 scenario period were determined from (a) the change of C content in the atmosphere, derived from the change in atmospheric CO_2 concentrations associated with the respective RCP (Meinshausen et al., 2011); (b) the previously published C exchange between ocean and atmosphere from IPSL-CM5A-LR RCP simulations ($F^{rcp}_{ocean,ipsl}$; Dufresne et al., 2013; Jones et al., 2013), which correspond to the modelled climate and CO_2 forcing used for the land model simulations (with the exception of a bias correction of the climatological mean); as well as (c) the land–atmosphere C exchange determined by the simulations s3 (RCP 8.5) and s4 (RCP 2.6; $F^{rcp}_{land,i}$).

$$E_i^{rcp} = k * \Delta C_A^{rcp} - F^{rcp}_{ocean,ipsl} - F^{rcp}_{land,i}, \quad (3)$$

where k (=2.12 Pg C/ppm) is the conversion factors of atmospheric CO_2 abundance to mass (Jones et al., 2013), and i is one particular ensemble member.

3 | RESULTS

3.1 | Present-day model performance

First we evaluate the ensemble with respect to its capacity to predict the present-day global C and N cycles in terms of overall stocks, gross fluxes and the net land–atmosphere C flux over the recent period (1996–2005 mean). The magnitude of the simulated net land–atmosphere C flux during the 1990s and 2000s, as well as the increment from the 1990s to the 2020s is within the range described in Le Quéré et al. (2018; GCP; see Figure 1), despite a somewhat stronger net C uptake of the ensemble compared to the Global Carbon Project (GCP) budget's multimodel mean and residual sink estimates. This net C uptake is associated with a simulated increase in terrestrial N storage of 23 ± 5 Tg N/year during 1996–2005 (unless otherwise stated numbers reported as mean and *SD* across ensemble members). At the global level, N constraints only slightly reduce gross primary production (GPP: 133 ± 9 Pg C/year vs. 138 Pg C/year for the C:N ensemble and C-only model respectively) and net primary production (NPP: 61 ± 4 Pg C/year vs. 62 Pg C/year). These numbers are broadly consistent with independent estimates (Beer et al., 2010; Saugier & Roy, 2001). Simulated global BNF ranges from 37 to 117 Tg N/year and thus accounts for most of the large literature range of plausible BNF estimates (Cleveland et al., 2013; Vitousek, Menge, Reed, & Cleveland, 2013), although one other study has suggested significantly larger rates (Xu-Ri & Prentice, 2017). The range of global N-use efficiency of vegetation production, that is the ratio of NPP to plant N uptake, is 46–66 g C/g N. A detailed overview of the model estimates is given in the Supporting Information (Table S1).

The limiting effect of N availability on C cycling in the ensemble is most prevalent polewards of 40° latitude, where the C–N ensemble shows lower productivity. For the Northern Hemisphere, this is in general terms in better agreement with independent data-driven estimates of gross primary productivity (Jung et al., 2011) than the C-only reference (Figure 2a,b). This finding is consistent with the comparison to atmospheric CO_2 observations (Figure 2c). Most ensemble members simulate the observed polewards increase of the seasonal cycle amplitude of atmospheric CO_2 concentrations (Ω_{lat}) better than the C-only reference. All ensemble members simulate the seasonal phasing and amplitude, as well as the sensitivity of

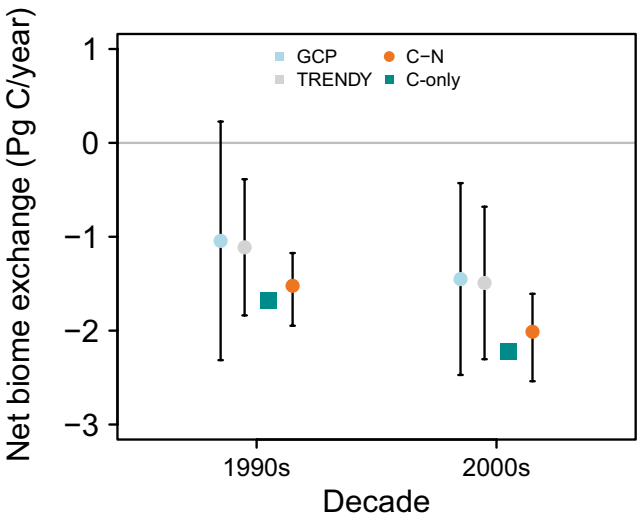

FIGURE 1 Comparison of simulated decadal land–atmosphere carbon exchange by the carbon–nitrogen ensemble (C–N) and the C-only reference (C-only) to estimates using a top-down budget estimate (Global Carbon Project [GCP]) and a bottom-up model ensemble (TRENDY) by the GCP (Le Quéré et al., 2018). Given are means, the error bars represent the range of the estimates

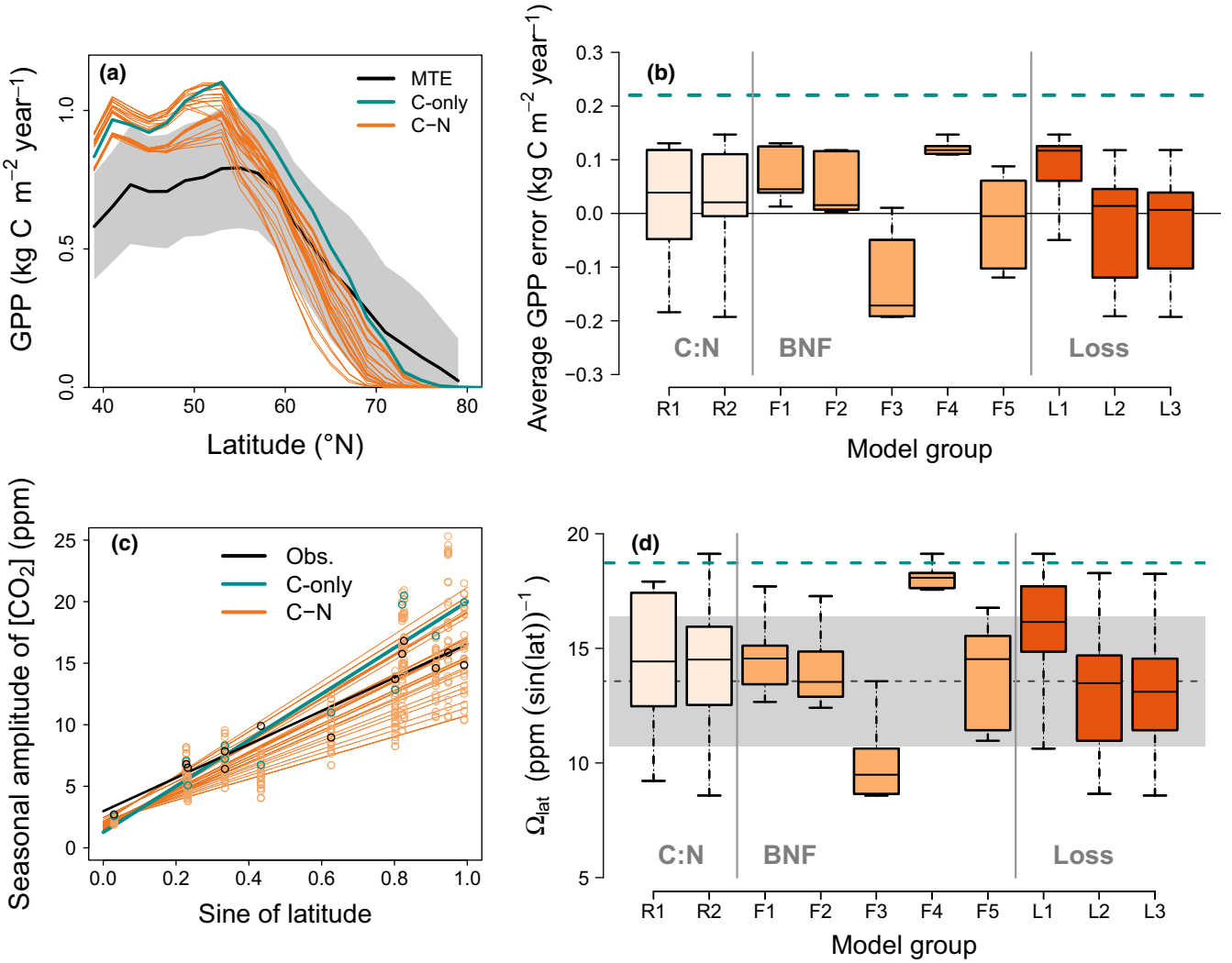

FIGURE 2 Comparison of contemporary mid- to high-latitude carbon cycle observations and ensemble predictions. (a) Average latitudinal gross primary productivity (GPP) between 40°N and 80°N (1982–2011 mean) based on empirical upscaling (multitree ensemble [MTE]; Jung et al., 2011, grey area indicates *SD*), the carbon–nitrogen ensemble members ('C–N') and the carbon-only reference ('C-only'). (b) Average error of model GPP predictions from panel (a). (c) 1982–2011 mean observed (black) and simulated seasonal CO_2 amplitudes (markers). Line fits indicate the latitudinal gradient of the seasonal CO_2 amplitudes (Table S2). (d) Modelled and measured (dashed black line and grey area, mean and *SD*) gradients of the northern hemispheric seasonal CO_2 amplitude (Ω_{lat}). In panels (b) and (d), boxes indicate quartiles around the median, and whiskers are the minimum and maximum values calculated by the carbon–nitrogen ensemble, with different shading indicating model groups. The dashed turquoise line shows the C-only prediction. See Supporting Information, Figure S1 for results of individual models. BNF, biological nitrogen fixation, C, carbon, N, nitrogen

atmospheric CO_2 to interannual climate variations (γ_{IAV}) largely in agreement with observations (Supporting Information, Figure S1 and Table S2).

The range of simulated present-day GPP and land C storage in tropical and temperate zones is affected by alternative assumptions about stoichiometry, where flexible stoichiometry (R2) generally allows for higher productivity and C storage. In mid- to high latitudes, where most of the model spread occurs, it is associated with the effect of alternative BNF algorithms (Figures 2b,d and 3), in particular by the effects of BNF algorithms F3 and F4 (Table 1). When BNF is calculated as a function of simulated evapotranspiration (BNF algorithm F3), low evapotranspiration in cold environments causes low rates of BNF. In turn, this reduces soil inorganic N availability and contributes to the underestimation of northern gross primary productivity. Conversely, when BNF is simulated primarily as a function of vegetation N demand (BNF algorithm F4), it occurs at a rate that mitigates the effects of N limitation on plant growth in cold environments. The resulting lack of a N constraint on leaf area development causes an overestimation of northern productivity similar to the C-only model.

3.2 | Future projections

Compared to the model spread during much of the 20th century, the spread in the ensemble predictions of the net land–atmosphere C flux

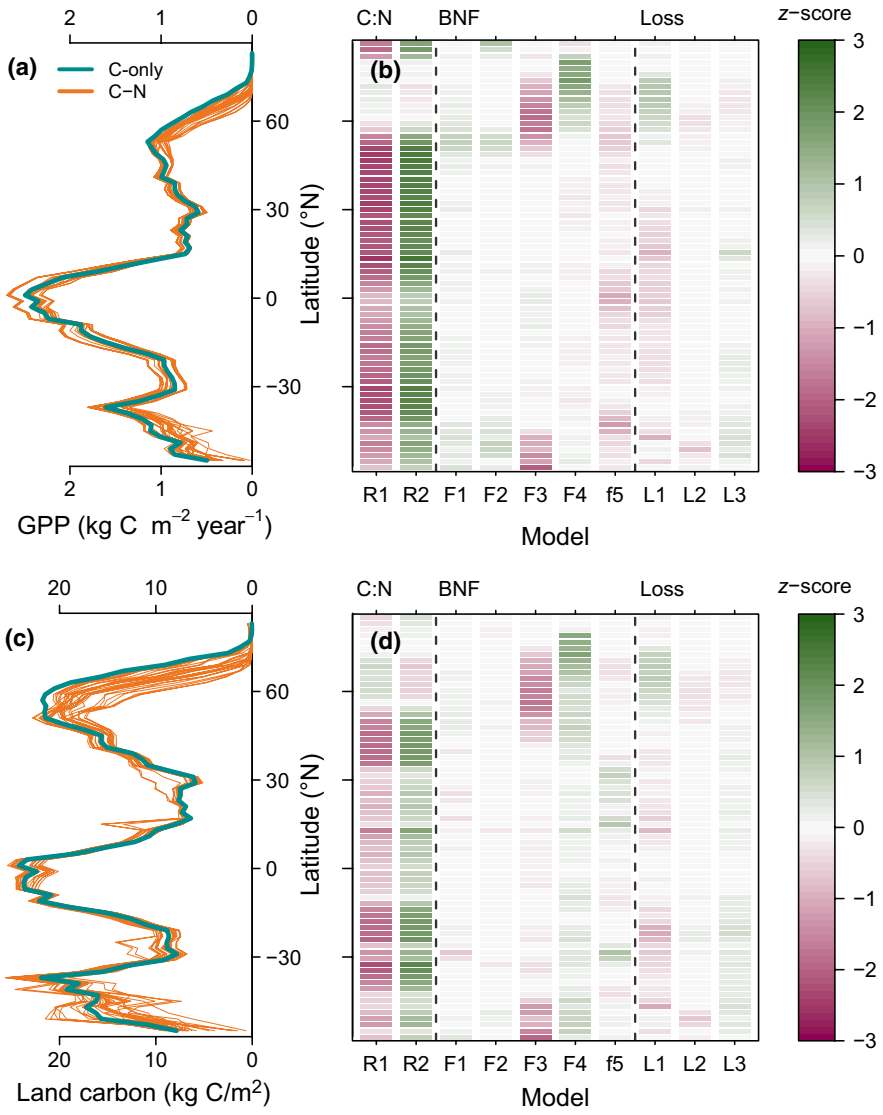

FIGURE 3 Simulated 1996–2005 average (a) gross primary productivity (GPP) and (c) land carbon storage along latitude. Panels (b) and (d) show the attribution of the effect of the different nitrogen-cycle algorithms as *z*-score (see Section 2.3.2 for details) on latitudinal GPP and land carbon storage respectively. Each model group includes all ensemble members with a particular nitrogen-cycle algorithm as described in Table 1

increases under both RCP scenarios during the first half of the 21st century (Figure 4a,b). The spread then declines again under RCP 2.6 as atmospheric CO_2 levels stabilize, whereas it continues to increase in the RCP 8.5 scenario with continuously growing atmospheric CO_2 levels (compare also Figure S2a). Integrated over the scenario period (2006–2099), N effects generally, but not always, reduce land C storage projections by 35 Pg C (70 Pg C decrease to 8 Pg C increase) for RCP 2.6 and by 72 Pg C (138 Pg C decrease to 31 Pg C increase) for RCP 8.5, compared to the C-only reference (195 Pg C for RCP 2.6; 336 Pg C for RCP 8.5). The effect of N on future C storage is strongest polewards of 40°N latitude in both hemispheres, where on average future C storage is reduced by 33 ± 18% (Figure 4c,d), and even stronger north of 55°N (46 ± 21%), whereas the effect is small in tropical latitudes (reduction of 4 ± 11%). As already shown in Figure 3, the uncertainty in mid- to high latitudes is dominated by the choice of BNF algorithms, in particular schemes F3 and F4. In tropical regions, the spread is further determined by the choice of C:N ratio algorithm. Flexible stoichiometry (scheme R2) generally allows for a stronger increase in future C storage (Figure 4e). The latitudinal distribution of the model spread and its attribution to different N-cycle algorithms is similar for both RCP scenarios, despite the differences in projected atmospheric CO_2 and climate change and the projected magnitude of C storage change (data not shown).

Underlying the projected changes in terrestrial C storage are changes in the terrestrial N cycle. Terrestrial C:N ratios are projected to increase by 11 ± 2% under RCP 2.6 and by 19 ± 3% under RCP 8.5, and thereby contribute to the future increase in land C storage (Figure 5a). This change in terrestrial stoichiometry results largely from an increased contribution of vegetation, mostly forest biomass with high C:N compared to forest soils, to total land C storage. For ensemble members with flexible C:N ratios (C:N algorithm R2), there is an additional but smaller decrease in tissue N concentrations due to elevated CO_2, leading to a small increase in terrestrial C:N ration (<1%) and a small effect in terms of overall C storage. Projections of changes in BNF range from a 5 Tg/year (10%) decrease to a 30 Tg N/year (50%) increase under RCP 2.6 and from a 3 Tg N/year (5%) decrease to a 60 Tg N/year (100%) increase under RCP 8.5 (Figure 5b). Ensemble members applying BNF algorithm F4 show by far the strongest increases in BNF

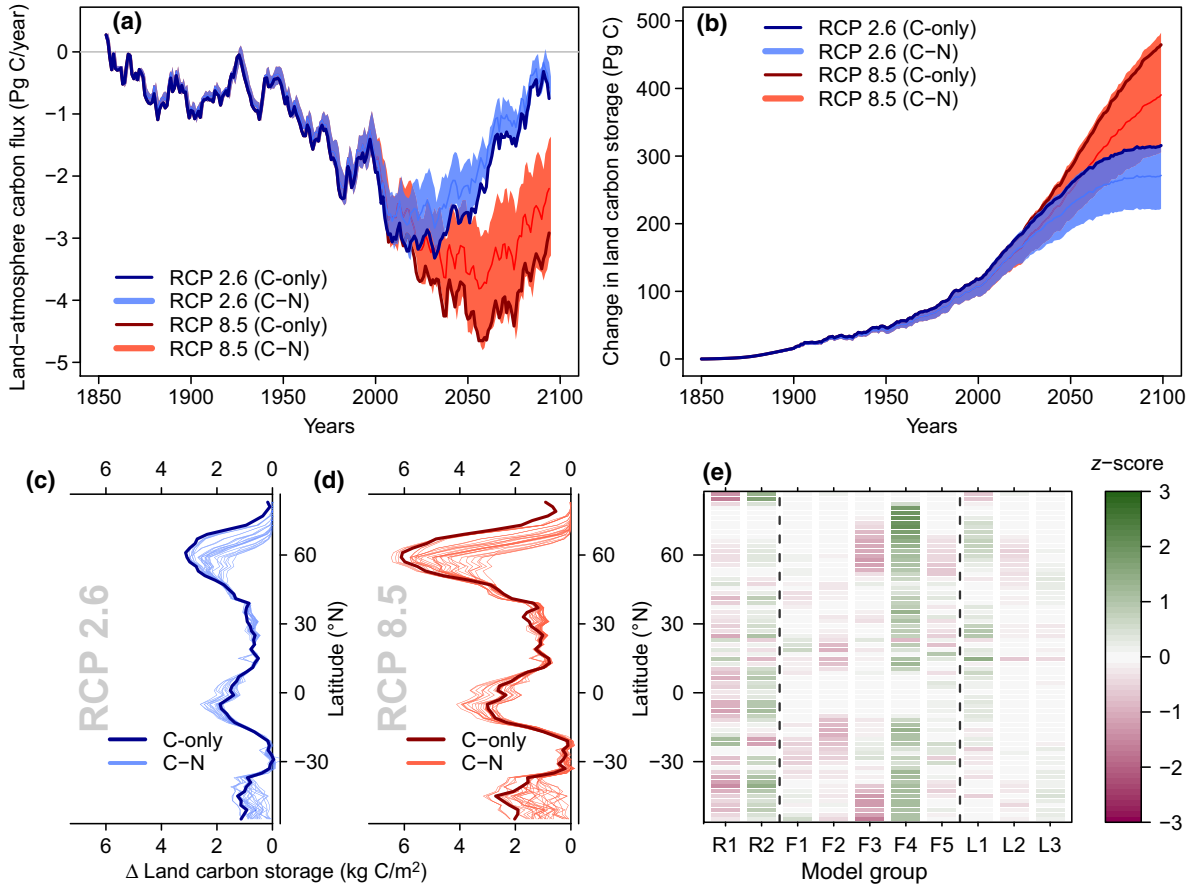

FIGURE 4 Projected net land–atmosphere carbon exchange under representative concentration pathways (RCPs) 2.6 and 8.5 scenarios of atmospheric CO_2 concentration, climate and nitrogen deposition. (a) 10-year running mean of the exchange for carbon–nitrogen ensemble projections as the mean (lines) and range (shaded area), as well as the predictions by the carbon-only reference. (b) Change in land carbon stock between 1850 and 2099. (c, d) Latitudinal mean change in land carbon between 2006 and 2099 under the RCP 2.6 and RCP 8.5 scenarios respectively. (e) Attribution of the effect of the different nitrogen-cycle algorithms as *z*-score (see Section 2.3.2 for details) on change in land carbon storage in the RCP 8.5 scenario. Each model group includes all ensemble members with a particular nitrogen-cycle algorithm as described in Table 1

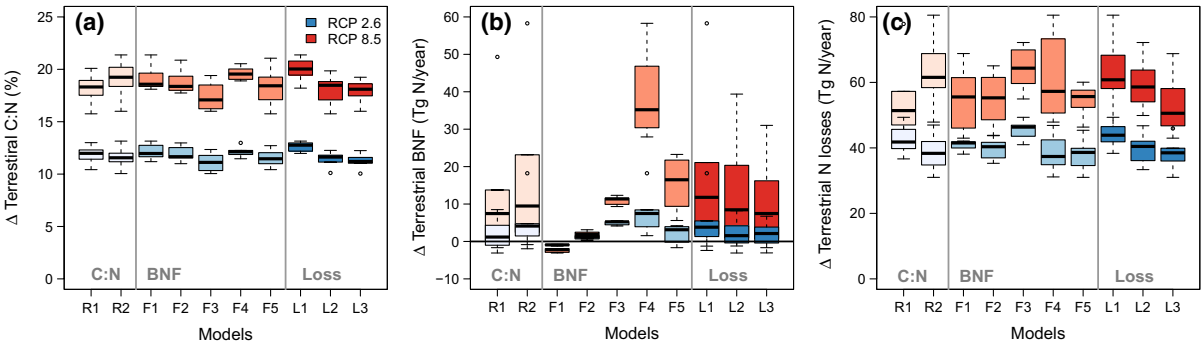

FIGURE 5 Projected globally integrated changes in (a) biosphere (soil organic matter, litter, vegetation) C:N ratio; (b) biological nitrogen fixation (BNF); and (c) nitrogen loss between the 1850s and the 2090s. Shown are simulation results over the common historical period (1850–2005), as well as the scenario periods (2006–2099) for representative concentration pathway (RCP) 2.6 (blue) and RCP 8.5 (red), with different shading indicating model groups. Note that N deposition increases in RCPs 2.6 and 8.5 contribute to the increased N losses independent of changes in BNF or internal nitrogen cycling. Model groups (n = 15, 6, 10 for the groups of carbon:nitrogen, BNF and N loss models) comprise all models in Table 1. See Figure S2 for time series of these changes

as N availability declines due to elevated CO_2. Consequently, the group of models that apply this algorithm predicts by far the largest amount of C sequestration between 2006 and 2099 (350 ± 20 Pg C *SD* within model group; 272 ± 34 Pg C for the group of all other models under RCP 8.5). These differences play out strongly under RCP 8.5 with continuously rising atmospheric CO_2, whereas near-constant atmospheric

CO_2 after the year 2030 in RCP 2.6 causes the model spread in net land–atmosphere CO_2 exchange to slowly decrease, as ensemble members with stronger N limitation gradually acquire the 'missing' N through increased BNF that outpaces N losses.

3.3 | Carbon-cycle sensitivities

To further understand the cause of the model spread in projected land C change from 1850 to 2099 under RCP 8.5, we decompose the projections in terms of their sensitivity to atmospheric CO_2 concentration increase, climate change and increased N deposition. The change in land C due to increasing atmospheric CO_2 concentrations, that is the C–concentration sensitivity β_L (Figure 6a,b) is the primary cause for the spread in projected land C storage change (Figure 4a). We find that N constraints reduce β_L in 29 out of 30 models (0.78 ± 0.15 Pg C/ppm, mean and *SD* across all CN models) compared to the C-only reference of 1.02 Pg C/ppm. This corresponds to an average reduction of β_L by 24 ± 15%. Ensemble members with a flexible stoichiometry (C:N algorithm R2) show a consistently larger response than members using fixed stoichiometry. Compared to a CO_2-related increase of only 5 ± 1% (mean ± *SD* difference between 1850 and 2099) simulated with assuming fixed C:N ratios (C:N algorithm R1), resulting from the increased contribution of woody vegetation to land C storage, allowing for flexible C:N ratios (C:N algorithm R2) increases vegetation C:N by 36 ± 12% in our ensemble. Another key factor in the model range is the spread in BNF responses to elevated CO_2. On average, the ensemble shows a sensitivity of BNF to increasing atmospheric CO_2 of 0.04 Tg N $year^{-1}$ ppm^{-1} (range: −0.01 to 0.21 Tg N $year^{-1}$ ppm^{-1}) for a CO_2 increase from 285 to 927 ppm between 1850 and 2099, with the lowest change in BNF scheme F3 and the largest change in scheme F4.

There is a tight correlation between the response of NPP to elevated levels of CO_2 and β_L (r^2 = .83, p < .01; Figure S3), because in the models, NPP is the primary driver of land C stock changes. An evaluation of the simulated, transient global NPP response to elevated CO_2 is challenging, because most experiments were done in artificial setting, for a short time and following a step-increase. It is nevertheless interesting to note that most C–N ensemble members show a global increase in NPP associated with the increase of atmospheric CO_2 from 350 to 550 ppm of 20.7 ± 3.6% (mean ± *SD*; C-only: 25.3%), which is consistent with a recent meta-analysis of total biomass responses to CO_2 enrichment experiments (22.3 [13.9%–31.4% 95% confidence range]; Baig et al., 2015), with only few C:N ensemble members showing a notably lower response.

The change of land C due to N deposition, that is the C–N sensitivity (η_L) averages 4.1 ± 2.2 Pg C/Pg N (Figure 6e,f). The range of this response is strongly affected by the choice of the stoichiometry algorithm. With flexible stoichiometry (algorithm R2), increasing N availability increases tissue N concentrations, leading on the one hand to higher photosynthesis and respiration rates per unit biomass, and on the other hand a higher N requirement for growth (see Meyerholt & Zaehle, 2015, for a more detailed discussion), which in combination reduces the C storage response to

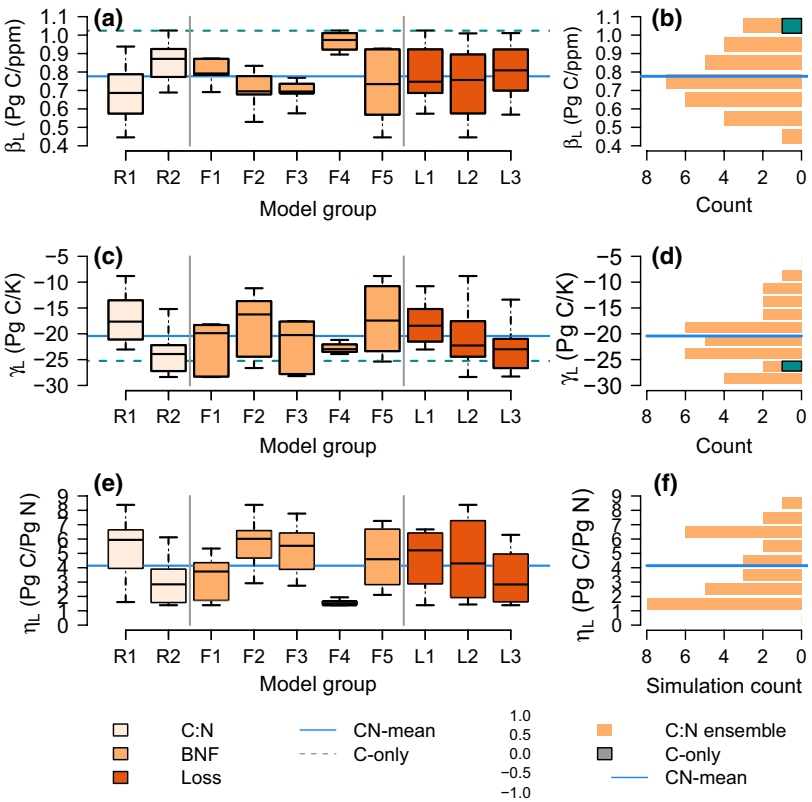

FIGURE 6 Sensitivity of simulated land carbon storage change (1850–2099) to changes in atmospheric CO_2 concentration (β_L), climate change (γ_L) and nitrogen deposition (η_L) under the representative concentration pathway 8.5 scenario. (a, c and e) The ensemble predictions of β_L, γ_L and η_L respectively. Boxes indicate median, quartiles and extreme values calculated by the carbon–nitrogen ensemble, with the shading indicating model groups. The blue line indicates the ensemble mean, dashed turquoise line the carbon-only reference. (b, d and f) The frequency distribution of β_L, γ_L and η_L, respectively, from the carbon–nitrogen ensemble and the carbon-only reference (turquoise block). The blue line indicates the carbon–nitrogen ensemble mean. Model groups (n = 15, 6, 10 for the groups of carbon:nitrogen, biological nitrogen fixation [BNF] and N loss models) comprise all models in Table 1

added N deposition. The simulated effect of increasing N deposition on vegetation C storage in the ensemble ranges 4.0 ± 7.8 Pg C/Pg N in tropical ecosystems, 8.2 ± 4.9 Pg C/Pg N in temperate forest ecosystems, and 16.6 ± 6.6 Pg C/Pg N in boreal ecosystems. This pattern broadly corresponds to that from the meta-analysis by Schulte-Uebbing and de Vries (2018; tropics: 1.3 [−1.3 to 3.9] Pg C/Pg N; temperate: 12.7 [10.6–14.9] Pg C/Pg N; boreal: 14.1 [10.6–17.5] Pg C/Pg N).

The change of land C due to climate change, that is the C–climate sensitivity (γ_L) averages −20 ± 5 Pg C/K (mean ± *SD*; Figure 6c,d), corresponding to a 19 ± 20% attenuation of the C losses simulated by the C-only reference (γ_L = −25 Pg C/K). This attenuation is primarily the result of N fertilization of vegetation due to enhanced soil N mineralization, which partially compensates increased for soil C losses as a result of increased soil respiration in a warmer world. Such an effect has been observed by one large-scale forest soil warming experiment (Magill et al., 2004), but the number of studies on full ecosystem warming effect on N cycling is too small to corroborate this effects at large scales. The attenuation is strongest with fixed stoichiometry (C:N algorithm R1) and N loss scheme L1. In the other two loss schemes, increased net mineralization directly results in an increase in ecosystem N losses through the assumption that a significant fraction of these losses are coupled to the net N mineralization rate, which prevents a larger fertilization effect.

A correlation between the C–climate sensitivity at centennial (γ_L) timescales and interannual (γ_{IAV}), apparent in the CMIP5 ESM ensemble (Cox et al., 2013), does not exist in our ensemble (Figure 7). The γ_{IAV} is similar between the C–N ensemble and the C-only reference, suggesting that the direct effects of interannual temperature variations on C cycle processes drive γ_{IAV} in the ensemble. Indirect effects resulting from temperature-related anomalies in N mineralization and plant uptake appear to play a lesser role at this timescale. The contribution of C:N and loss algorithms to the uncertainty in γ_L clearly indicates that these processes contribute notably to the long-term climate response of the biosphere (Figure 6). This finding suggests that the correlation in the CMIP5 ensemble may be a result of the simplified model structure considered, and may be altered when the long-term effects of nutrient-related soil-vegetation feedbacks on the response of ecosystems to perturbations are taken into account.

In the ensemble, β_L is highly anti-correlated with the sensitivity of terrestrial C storage to N deposition η_L (r^2 = .89, p < .01; Figure 8). This correlation reflects the differing degree of N limitation in the ensemble: ensemble members with low present-day N availability and therefore low productivity (Figure 2) are more sensitive to N added from deposition, and at the same time also more limited in their ability to respond to CO_2 fertilization with increased production and C storage. Ensemble members with strong simulated N limitation (low response to elevated CO_2) also retain more ecosystem C in a warmer climate through a larger fertilization effect from warming-induced increases in net N mineralization. Consequently, γ_L in the C–N ensemble is weakly anti-correlated with β_L (r^2 = .56, p < .01) and positively correlated with the sensitivity of land C storage to N deposition η_L (r^2 = .65, p < .01).

The correlation between the C cycle sensitivities suggest that there is a compensation of uncertainty in terms of future land C storage in N-enabled models. To assess the magnitude of this effect, we evaluated Equation (3) for the range of β_L, γ_L and η_L in the ensemble, but assuming no correlation between them. This simple propagation of errors of the mean yields a change in total land C between 1850 and 2099 of 382 ± 109 Pg C, compared to the spread in the ensemble (382 ± 53 Pg C). This reduction in the model spread by more than half through the interactions of N cycle

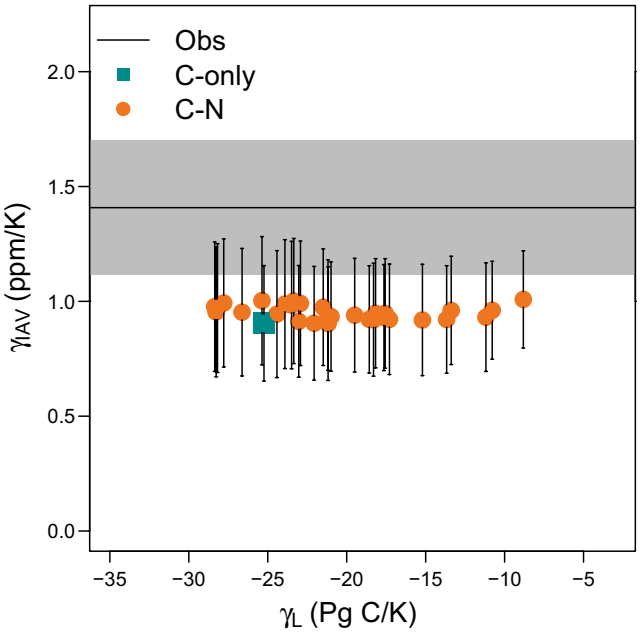

FIGURE 7 Correlation between the land climate sensitivity γ_L and the response of the atmospheric CO_2 growth rate to interannual climate variability γ_{IAV}

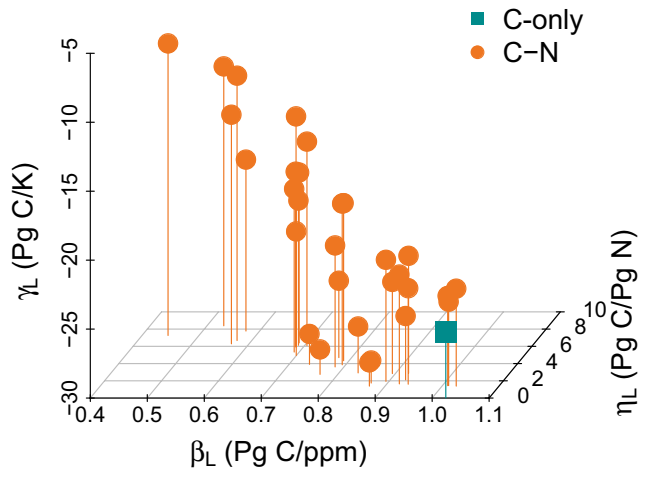

FIGURE 8 Correlation of the sensitivity of simulated land carbon storage change (1850–2099) to changes in atmospheric CO_2 concentration (β_L), climate change (γ_L) and nitrogen deposition (η_L) under the representative concentration pathway 8.5 scenario

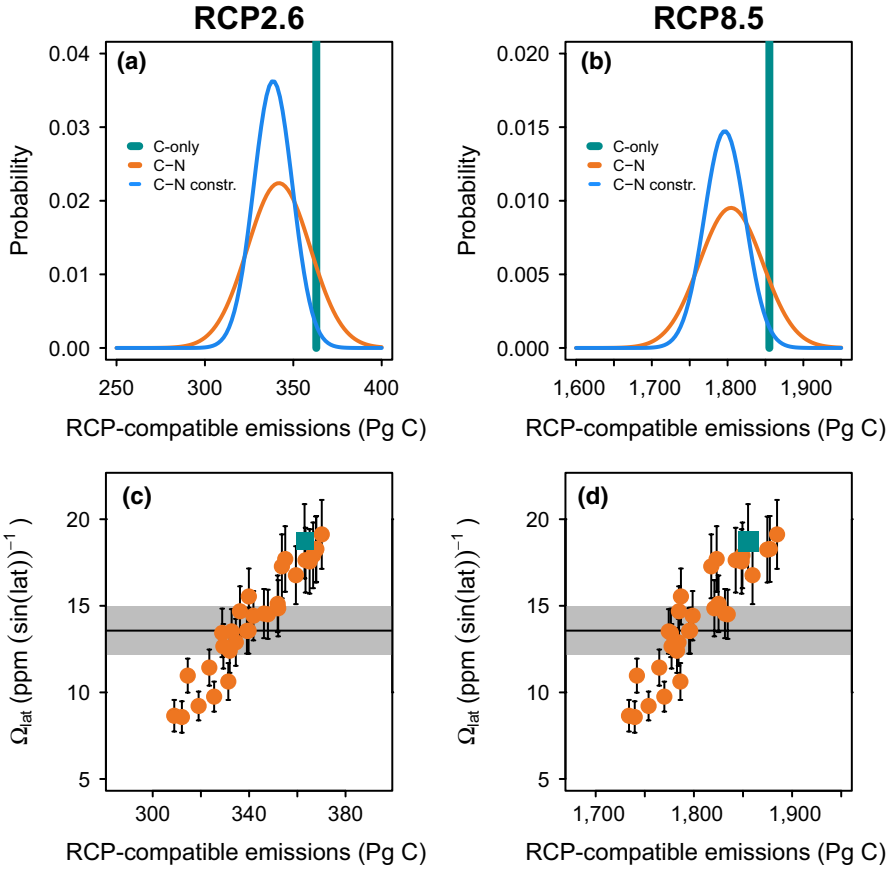

FIGURE 9 Estimates of anthropogenic CO_2 emissions (2006–2099) compatible with the representative concentration pathway (RCP) 2.6 and RCP 8.5 climate change scenarios. (a) Probability distribution functions representing the carbon–nitrogen ensemble predictions (orange curve) under RCP 2.6, as well as the distribution constrained by ensemble member performance against the atmospheric constraint Ω_{lat} (blue curve). The turquoise line indicates the prediction of the carbon-only reference. (b) Same as panel a for RCP 8.5. (c, d) The correlation between RCP-compatible emissions and the slope of the increase in the CO_2 seasonal cycle with latitude Ω_{lat}, used for model weighting. See Figure S4 for derivation of the frequency distributions for the unconstrained ensemble, and the Supporting Information for the model weighting to derive the constrained probability distribution

processes highlights the need to account explicitly for these processes and their effect on C cycling in assessments of future biosphere dynamics.

3.4 | RCP-compatible anthropogenic CO_2 emissions

We lastly assess the impact of the projected land C uptake on future anthropogenic CO_2 emission pathways that are compatible with the representative CO_2 concentration pathways of the RCP scenarios. When the N effect is taken into account, the predicted compatible emissions for the 2006–2099 period are reduced to 342 ± 18 Pg C (mean ± *SD*) for RCP 2.6 and 1,805 ± 42 Pg C for RCP 8.5, compared to the C-only reference of 371 Pg C for RCP 2.6 and 1,863 Pg C for RCP 8.5 (Figure 9).

The estimates of RCP-compatible emissions are strongly correlated with the present-day latitudinal distribution of productivity (Figure 9), as measured by Ω_{lat} (as defined in Figure 2; RCP 2.6: r^2 = .92; RCP 8.5: r^2 = .91). Using the Ω_{lat} constraint to weight ensemble member predictions (see Supporting Information) slightly decreases the mean estimate and range of RCP-compatible emissions (Figure 9), but the effect is much lower than in a previous study based on C-cycle-only models owing to the larger spread in their ensemble (Booth et al., 2017). For RCP 2.6, our ensemble estimate of RCP-compatible emissions under N constraints is 339 ± 11 Pg C (mean ± *SD*), a reduction from the C-only estimate by 32 Pg C or 9%. For RCP 8.5, we predict RCP-compatible emissions of 1,796 ± 28 Pg C, a reduction relative to the C-only reference by 67 Pg C or 4%.

4 | DISCUSSION

In this paper, we analysed future projections of the terrestrial C cycle using an ensemble of 30 C–N cycle models with alternative representations of C–N stoichiometry, BNF and N losses. We find that the ensemble is generally within or at least close to the range of observations with respect to contemporary global C-cycle benchmarks. Our consistent framework combining alternative model process representation elucidates the otherwise hidden consequence of model assumptions and thereby provides a more robust estimate of the N constraints on future C budget compared to previous studies (Wieder, Cleveland, Smith, et al., 2015; Zaehle et al., 2015; Zhang et al., 2014). Based on this analysis, we find that N dynamics reduce the global CO_2 fertilization effect under the RCP 8.5 scenario by 24 ± 15% and reduce the C loss associated with global warming by 19 ± 20%. In combination, the result is a reduction of projected land C storage under the RCP 8.5 scenario of 21% (−9% to +41%). The relative reduction in future land C uptake is slightly lower in the climate change stabilization scenario RCP 2.6, where it averages 19% (−3% to 40%). Integrated assessment models that are used to calculate the compatible emissions based on ocean and land C uptake do currently not account for terrestrial N dynamics. The results of our study suggest that an additional mitigation effort is

required to maintain atmospheric CO_2 at levels prescribed in the RCP scenarios of 9 ± 3% (RCP 2.6) and 4 ± 2% (RCP 8.5).

Previous studies (Sokolov et al., 2008; Thornton et al., 2009; Zaehle, Friedlingstein, et al., 2010) have suggested ranges for the C–concentration sensitivity (β_L) in N-enabled models between 0.6 and 1.2 Pg C/ppm, which includes our best estimate of 0.75 ± 0.13 Pg C/ppm (mean ± *SD*). A direct comparison of these estimates is challenging as they are known to be scenario dependent (Arora et al., 2013). In terms of the relative reduction of β_L compared to a C-only model version, which ranged 50% and 80% (Sokolov et al., 2008; Thornton et al., 2009; Wårlind et al., 2014), we find a smaller reduction due to the inclusion of N cycling (24 ± 15%). Our quantification of the C–climate sensitivity (γ_L) is also consistent with previous studies (Sokolov et al., 2008; Thornton et al., 2009; Wårlind et al., 2014; Zaehle, Friedlingstein, et al., 2010). In all these models, N interactions partly mitigated the positive C–climate feedback because N mineralization from SOM decomposition fertilizes plant growth in N-limited ecosystems and thus leads to enhanced vegetation C storage. However, none of the ensemble members showed a shift to a negative feedback, as suggested by the CLM4 model (Thornton et al., 2009).

4.1 | Process attribution

One advantage of our ensemble approach is that it enables direct attribution of ensemble uncertainty to process formulations (Figures 2–6). The comparison demonstrates that alternative model choices of each of the processes considered have characteristic and important implications for the simulated level of present-day and future N limitation. Our analysis demonstrates further that in combination, these three process formulations capture a wide range of C–N cycle interactions: for instance, assuming a combination of a vegetation N demand-driven BNF (BNF algorithm F4), a flexible stoichiometric constraint on growth (C:N algorithm R2), as well as a hierarchical N loss scheme (L3) leads to a model with prognostic N cycle that has little constraining effect on the decadal to centennial C-cycle projections. Conversely, assuming tight stoichiometric constraints (C:N algorithm R1), direct dependence of BNF on N-limited plant production or CO_2-sensitive evapotranspiration (BNF algorithms F2 and F3 respectively), as well as a concentration-based N loss scheme (L1) results in a comparatively strong N limitation effect, but still does not reproduce the very strong N limitation suggested initially by CLM4 (Thornton et al., 2009). Our regional analysis further reveals that different processes are important in different locations/climates, illustrating the regional nature of simulated N limitation.

In the ensemble, the BNF response to elevated CO_2 is the largest source of uncertainty. This reflects the relatively poor understanding of the processes, and their representation in models, affecting BNF at large scale. Increases in response to CO_2 have been observed in controlled experiments (e.g. between 30% and 62% in a recent meta-analysis by Liang, Qi, Souza, & Luo, 2016), but the responses were low or declining over time due to other limiting factors (Hofmockel & Schlesinger, 2007; Hungate et al., 2003, 2004). Two BNF schemes stand out in their CO_2 response: coupling BNF to evapotranspiration (BNF algorithm F3) leads to the geographically wide-spread prediction that BNF decreases in response to CO_2 by about 7 Tg N/year or 7% globally, despite increasing N limitation of plant growth. Such a behaviour does not appear to be supported by the available evidence. Conversely, assuming a BNF dependence on instantaneous vegetation N demand and light availability (BNF algorithm F4) leads to a large projected increase of BNF (on average by 126 Tg N/year or 208% between 1850 and 2099) in response to increasing CO_2, particularly in temperate and boreal regions. While such a demand-driven approach appears to be appealing from a process understanding perspective, its current implementation lacks sufficient representation of other limiting factors for the BNF response. Removing these two BNF algorithms F3 and F4 from the ensemble changes projected 1860–2099 land C storage only slightly, although it reduces the uncertainty in the ensemble: the projected land C storage for RCP 8.5 (RCP2.6) of 384 ± 52 (265 ± 28) Pg C is reduced to 379 ± 39 (263 ± 21). Understanding the global patterns of BNF, as well as its environmental controls in response to changing C and nutrient availability should therefore be a priority in reducing N-related uncertainty (see e.g. Zheng, Zhou, Luo, Zhao, & Mo, 2019). Furthermore, all algorithms considered in our study have in common that they do not consider community assembly and dynamics as part of the processes that constrain BNF responses and only relate BNF to instantaneous changes in ecosystem N properties. It will likely be necessary to explicitly represent the effects of community dynamics and assembly to represent the timescale of BNF shifts at ecosystem level (Menge, Hedin, & Pacala, 2012; Menge, Levin, & Hedin, 2008; Thomas et al., 2015).

The choice of fixed versus flexible C:N ratios contribute to variations in our estimates of both β_L and γ_L. Assuming fixed stoichiometry leads to a tighter N constraint and thus a more profound impact on the CO_2 and climate response. With flexible stoichiometry (algorithm R2) increasing N availability increases tissue N concentrations, and vice versa. Increased tissue N concentrations lead on the one hand to higher photosynthesis and respiration rates per unit biomass, and on the other hand a higher N requirement for growth (see Meyerholt & Zaehle, 2015, for a more detailed discussion), which in combination reduces the C storage response to added N. While some flexibility has been observed (Ainsworth & Long, 2005; Magill et al., 2004; McNulty et al., 2005), recent model-data intercomparison studies have suggested that it is overestimated by current model formulations (Meyerholt & Zaehle, 2015; Zaehle et al., 2014), clearly demonstrating the need for a better representation of this process. However, the impact of stoichiometric flexibility on overall land C sequestration considering all forcings is attenuated because of the compensating effects of climate warming and N deposition on plant N availability, and the large share of low C:N SOM pools with limited stoichiometric flexibility in the total land C storage. Therefore, although important from a process representation point of view, the overall contribution to land C storage trends is small compared to that of BNF in our study.

The N loss formulation does not have a clear effect on the biospheric response to elevated CO_2, but shows a strong impact on the climate sensitivity of the C cycle (γ_L, Figure 6c). The assumption that ecosystem N loss is primarily controlled by the rate of soil N turnover (loss algorithms L2 and L3) leads to higher predicted soil N losses in response to warming. In these cases, vegetation has limited potential to act as a N sink, leading to a lower fertilization effect compared to loss algorithm L1 (Figure 6c). In particular, we found that a combination of flexible stoichiometry and the hierarchical N loss scheme (algorithm L3) leads to climate-induced C losses that are comparable to those simulated by the C-cycle only version of the model. The effect of increased N availability leads to a decline in vegetation C:N with C:N algorithm R2, compared to a slight increase when assuming time-invariant C:N (C:N algorithm R1), and thereby attenuates the fertilization response. Thus far, N-loss algorithms in TBMs are largely unconstrained by observations, despite some attempts to evaluate simulated N_2O fluxes (e.g. Tian et al., 2019; Xu-Ri & Prentice, 2008; Zaehle et al., 2011). When assessing different loss algorithms, feedbacks in the simulated C and N cycles can lead to equifinality with respect to C cycle observations (Meyerholt & Zaehle, 2018). In order to better constrain N loss process parameterization, there is a need for ecosystem-scale experiments or monitoring studies that focus on quantification of the relevant N-loss pathways and their systematic use for model evaluation. An alternative source of information may be linked to the use of ^{15}N abundance data, which could be used both in a process-based manner by comparison to ^{15}N enrichment studies providing insight into the fate of N in terrestrial ecosystems (Goodale, 2017), or by attempting to interpret spatial and or temporal trends of ^{15}N abundance in terms of changes in the terrestrial N cycle (Craine et al., 2018, 2019; Hiltbrunner, Körner, Meier, Braun, & Kahmen, 2019; Houlton, Marklein, & Bai, 2015).

4.2 | Limitations of the study

Further alternative process representations in current N-enabled TBMs exist, for example the competition of plants and soil organisms for N or the downregulation of photosynthesis (Zaehle & Dalmonech, 2011). These additional processes would likely increase the effect of the internal (C:N) versus external N cycle (N in- and output) uncertainty, but are unlikely to affect our conclusions on the importance of BNF and N loss process representations, given the magnitude of the projected change particularly in BNF and the long timescale at which these changes occur. One process only implicitly considered in the ensemble of this study is nutrient mining in response to increased below-ground C allocation under elevated CO_2. In the ensemble, models with flexible C:N stoichiometry allow for a redistribution of N from soil to vegetation under N stress, because of increasing SOM C:N ratios. However, this process has been insufficient to explain the observed redistribution of soil N to the vegetation in free-air CO_2 enrichment experiments at Duke and ORNL forest (Zaehle et al., 2014). Increased below-ground C allocation has been found to increase SOM turnover (Drake et al., 2013; Hungate et al., 2009), and has been hypothesized to contribute to the sustained response of N-limited forests to elevated CO_2 in ecotomycorrhizal-dominated forests (Norby et al., 2017; Terrer, Vicca, Hungate, Phillips, & Prentice, 2016). One recent global model accounting for this effect suggested a substantial redistribution effect of N, essentially increasing land C storage, as increased soil C losses are more than compensated by increased above-ground C storage following this indirect fertilization effect (Sulman et al., 2019). This could potentially alter our conclusion about the importance of BNF in determining future N limitation in favour of processes determining ecosystem internal N cycling.

The absolute values of land C uptake and its sensitivities to environmental drivers depend on the C cycle assumptions built into O-CN. Nevertheless, we believe that the insights into sign and magnitude of the N cycle process contributions (Figure 6) will be transferrable to other TBMs. Each of the N process algorithms applied in this study (Table 1) relies on few, insufficiently constrained parameters. We chose the parameter values in accordance with previous work (Meyerholt & Zaehle, 2015, 2018; Meyerholt et al., 2016), which resulted in flux and stock magnitudes after model spin-up commensurate with current understanding (Supporting Information, Table S1). The simulated process responses to perturbations may be sensitive to the precise parameterization of the algorithms. Therefore our ensemble range may be a conservative estimate of the full N cycle uncertainty range. Considering that most algorithms respond linearly to small parameter perturbations (e.g. Meyerholt et al., 2016), it is unlikely that this uncertainty will affect the general conclusions drawn here about the relative importance and sign of the individual process contributions or the overall sign and range of the N effect.

As many other studies (Arora et al., 2019), this study does not consider the limitation of the terrestrial C cycle by the phosphorus (P) cycle. A first field-scale free-air CO_2 enrichment experiment in an Australian Eucalypt forest with low P availability has shown that P limitation can severely constrain the response (Ellsworth et al., 2017). Model simulations made for this and a planned experiment in the P-limited Amazon rain forests have demonstrated that the effect of P availability can be much stronger than N effects in P-limited ecosystems, but large uncertainties persist in these simulations (Fleischer et al., 2019; Medlyn et al., 2016). Considering P in addition to N dynamics in our ensemble would likely result in attenuated CO_2 responses in predominantly P-limited ecosystems, such as the Amazon rain forest or large parts of Australia.

4.3 | Model evaluation

We evaluated the model ensemble against a range of contemporary C-cycle observations, and demonstrated good, but varying performance of the ensemble members. In our ensemble, the difference in high-latitude productivity results directly from N cycle processes, as the C-cycle only reference considered all other climate

constraints but the N cycle. The larger than observed high-latitude productivity of the C-cycle control may be O-CN specific, and could likely be corrected without necessarily including a fully prognostic N cycle. The variable performance of current C-cycle models and C–N cycle models (Le Quéré et al., 2018) suggest that currently, these benchmarks cannot be conclusively used to demonstrate that N cycle representations are necessary to match contemporary observations. However, they do allow us to state that all ensemble members in our study represent terrestrial C–N dynamics to a degree comparable to other state-of-the-art in biosphere models and that they are therefore valid candidates to assess potential future biosphere dynamics.

Despite the good present-day performance, substantial spread remains in the projected N effect on future land C sequestration. These results support the concept of an ensemble approach to make a more robust assessment about the likely effect of N on projections of the global C cycle. The results further imply that advanced global C-cycle benchmarking systems (Collier et al., 2018; Righi et al., 2019) may insufficiently constrain long-term dynamics of the terrestrial biosphere, as they do not sufficiently constrain N availability and its effect on terrestrial C cycling. However, we note that we have not fully exploited the available observations. In our ensemble, some of the uncertainty resides in high-latitude ecosystems. Applying regionally explicit benchmarks, such as satellite-derived estimates of vegetation C (Liu, Dijk, McCabe, Evans, & Jeu, 2013) would likely help to constrain the model spread better. However, these data would not directly constrain simulated N dynamics, but other model features more directly affecting vegetation turnover.

Reducing uncertainty in the N effect requires the development of adequate and robust constraints on the terrestrial N cycle and its effect on vegetation growth and SOM decomposition, which necessarily requires a multifaceted approach. There is a need to improve the general understanding of ecosystem N dynamics and their covariation with C and water fluxes through a systematic observation and reporting of relevant N cycle characteristics in ecosystem monitoring to fully make use of the available C cycle observations to constrain coupled C–N cycle models (e.g. Vicca et al., 2018). A complementary source of information could be obtained by testing the simulated covariation of plant stoichiometry with climate and soils within plant functional types using existing plant trait databases (e.g. Kattge et al., 2011). The increasing availability of hyperspectral remote sensing will provide a new tool to better evaluate regional trends in foliar N content or related leaf properties (Croft et al., 2020; Knyazikhin et al., 2013; Ollinger et al., 2008; Townsend, Serbin, Kruger, & Gamon, 2013).

However, the evaluation of biosphere models with observations from monitoring networks will always and unavoidably be confounded by co-occurring effects of global change which obscure the effects of C–N coupling. It will therefore remain important to perform hypothesis-driven model evaluation against manipulation experiments to test model formulations with respect to those processes that determine the mid- to long-term response of ecosystems to perturbations (Medlyn et al., 2015), potentially involving new field experimentation dedicated to understanding the long-term response of ecosystems to changes in C or N availability (Norby et al., 2016). Even with improved constraints on current terrestrial N dynamics, the divergence of simulation results over the 21st century suggests that the long-term effect of N dynamics will remain to some extend unconstrained by current observations. This highlights the need for an ensemble approach to adequately reflect uncertainties in our process understanding in projections of the future C cycle.

DATA AVAILABILITY STATEMENT

Globally aggregated output of the ensemble is available at doi: https://doi.org/10.5281/zenodo.3620826. The O-CN model code is available from the authors upon request.

ACKNOWLEDGEMENTS

The authors acknowledge funding from the European Union's Horizon 2020 research and innovation programme (grant agreement no. 641816; CRESCENDO), as well as the European Research Council (ERC; grant agreement no. 647204; QUINCY).

AUTHOR CONTRIBUTION

J.M. and S.Z. designed the study and performed the analysis; J.M. implemented, tested and calibrated the models; S.Z. and K.S. performed the simulations. All the authors contributed to the writing.

ORCID

Sönke Zaehle https://orcid.org/0000-0001-5602-7956

REFERENCES

Ainsworth, E. A., & Long, S. P. (2005). What have we learned from 15 years of free-air CO_2 enrichment (FACE)? A meta-analytic review of the responses of photosynthesis, canopy properties and plant production to rising CO_2. *New Phytologist*, *165*, 351–372. https://doi.org/10.1111/j.1469-8137.2004.01224.x

Arora, V. K., Boer, G. J., Friedlingstein, P., Eby, M., Jones, C. D., Christian, J. R., … Wu, T. (2013). Carbon-concentration and carbon-climate feedbacks in CMIP5 Earth system models. *Journal of Climate*, *26*, 5289–5314. https://doi.org/10.1175/JCLI-D-12-00494.1

Arora, V. K., Katavouta, A., Williams, R. G., Jones, C. D., Brovkin, V., Friedlingstein, P., … Chamberlain, M. A. (2019). Carbon-concentration and carbon-climate feedbacks in CMIP6 models, and their comparison to CMIP5 models. *Biogeosciences Discussions*, 1–124. https://doi.org/10.5194/egusphere-egu2020-6124

Baig, S., Medlyn, B. E., Mercado, L. M., & Zaehle, S. (2015). Does the growth response of woody plants to elevated CO_2 increase with temperature? A model-oriented meta-analysis. *Global Change Biology*, *21*, 4303–4319. https://doi.org/10.1111/gcb.12962

Beer, C., Reichstein, M., Tomelleri, E., Ciais, P., Jung, M., Carvalhais, N., … Papale, D. (2010). Terrestrial gross carbon dioxide uptake: Global distribution and covariation with climate. *Science*, *329*, 834–838. https://doi.org/10.1126/science.1184984

Boden, T., Marland, G., & Andres, R. (2013). *Global, regional, and national fossil-fuel CO_2 emissions*. Oak Ridge, TN: Carbon Dioxide Information Analysis Center, Oak Ridge National Laboratory, US Department of Energy. https://doi.org/10.3334/CDIAC/00001_V2016

Booth, B. B. B., Harris, G. R., Murphy, J. M., House, J. I., Jones, C. D., Sexton, D., & Sitch, S. (2017). Narrowing the range of future

climate projections using historical observations of atmospheric CO_2. *Journal of Climate*, *30*, 3039–3053. https://doi.org/10.1175/JCLI-D-16-0178.1

Cleveland, C. C., Houlton, B. Z., Smith, W. K., Marklein, A. R., Reed, S. C., Parton, W. J., & Running, S. W. (2013). Patterns of new versus recycled primary production in the terrestrial biosphere. *Proceedings of the National Academy of Sciences of the United States of America*, *110*(31), 12733–12737. https://doi.org/10.1073/pnas.1302768110

Cleveland, C. C., Townsend, A. R., Schimel, D. S., Fisher, H., Howarth, R. W., Hedin, L. O., … Wasson, M. F. (1999). Global patterns of terrestrial biological nitrogen (N-2) fixation in natural ecosystems. *Global Biogeochemical Cycles*, *13*, 623–645. https://doi.org/10.1029/1999gb900014

Collier, N., Hoffman, F. M., Lawrence, D. M., Keppel-Aleks, G., Koven, C. D., Riley, W. J., … Randerson, J. T. (2018). The international land model benchmarking (ILAMB) system: Design, theory, and implementation. *Journal of Advances in Modeling Earth Systems*, *10*, 2731–2754. https://doi.org/10.1029/2018MS001354

Cox, P. M., Pearson, D., Booth, B. B. B., Friedlingstein, P., Huntingford, C., Jones, C. D., & Luke, C. M. (2013). Sensitivity of tropical carbon to climate change constrained by carbon dioxide variability. *Nature*, *494*, 341–344. https://doi.org/10.1038/nature11882

Craine, J. M., Elmore, A. J., Wang, L., Aranibar, J., Bauters, M., Boeckx, P., … Zmudczyńska-Skarbek, K. (2018). Isotopic evidence for oligotrophication of terrestrial ecosystems. *Nature Ecology & Evolution*, *2*, 1735–1744. https://doi.org/10.1038/s41559-018-0694-0

Craine, J. M., Elmore, A. J., Wang, L., Boeckx, P., Delzon, S., Fang, Y., … Werner, C. (2019). Reply to: Data do not support large-scale oligotrophication of terrestrial ecosystems. *Nature Ecology & Evolution*, *3*, 1287–1288. https://doi.org/10.1038/s41559-019-0949-4

Croft, H., Chen, J., Wang, R., Mo, G., Luo, S., Luo, X., … Bonal, D. (2020). The global distribution of leaf chlorophyll content. *Remote Sensing of Environment*, *236*, 111479. https://doi.org/10.1016/j.rse.2019.111479

Dalmonech, D., & Zaehle, S. (2013). Towards a more objective evaluation of modelled land-carbon trends using atmospheric CO_2 and satellite-based vegetation activity observations. *Biogeosciences*, *10*, 4189–4210. https://doi.org/10.5194/bg-10-4189-2013

Drake, J. E., Darby, B. A., Giasson, M. A., Kramer, M. A., Phillips, R. P., & Finzi, A. C. (2013). Stoichiometry constrains microbial response to root exudation- insights from a model and a field experiment in a temperate forest. *Biogeosciences*, *10*, 821–838. https://doi.org/10.5194/bg-10-821-2013

Du, Z., Weng, E., Jiang, L., Luo, Y., Xia, J., & Zhou, X. (2018). Carbon–nitrogen coupling under three schemes of model representation: A traceability analysis. *Geoscientific Model Development*, *11*, 4399–4416. https://doi.org/10.5194/gmd-11-4399-2018

Dufresne, J.-L., Foujols, M.-A., Denvil, S., Caubel, A., Marti, O., Aumont, O., … Vuichard, N. (2013). Climate change projections using the IPSL-CM5 Earth System Model: From CMIP3 to CMIP5. *Climate Dynamics*, *40*, 2123–2165. https://doi.org/10.1007/s00382-012-1636-1

Ellsworth, D. S., Anderson, I. C., Crous, K. Y., Cooke, J., Drake, J. E., Gherlenda, A. N., … Reich, P. B. (2017). Elevated CO_2 does not increase eucalypt forest productivity on a low-phosphorus soil. Nature. *Climate Change*, *7*, 279–282. https://doi.org/10.1038/nclimate3235

Field, C. B., & Mooney, H. (1986). The photosynthesis-nitrogen relationship in wild plants. In T. J. Givnish (Ed.), *On the economy of plant form and function* (pp. 25–55). Cambridge, UK: Cambridge University Press. ISBN 0521022495.

Fleischer, K., Rammig, A., De Kauwe, M. G., Walker, A. P., Domingues, T. F., Fuchslueger, L., … Lapola, D. M. (2019). Amazon forest response to CO_2 fertilization dependent on plant phosphorus acquisition. *Nature Geoscience*, *12*, 736–741. https://doi.org/10.1038/s41561-019-0404-9

Gerber, S., Hedin, L. O., Oppenheimer, M., Pacala, S. W., & Shevliakova, E. (2010). Nitrogen cycling and feedbacks in a global dynamic land model. *Global Biogeochemical Cycles*, *24*, GB1001. https://doi.org/10.1029/2008GB003336

Goll, D. S., Brovkin, V., Parida, B. R., Reick, C. H., Kattge, J., Reich, P. B., … Niinemets, Ü. (2012). Nutrient limitation reduces land carbon uptake in simulations with a model of combined carbon, nitrogen and phosphorus cycling. *Biogeosciences*, *9*, 3547–3569. https://doi.org/10.5194/bg-9-3547-2012

Goodale, C. L. (2017). Multiyear fate of a ^{15}N tracer in a mixed deciduous forest: Retention, redistribution, and differences by mycorrhizal association. *Global Change Biology*, *23*, 867–880. https://doi.org/10.1111/gcb.13483

Gruber, N., & Galloway, J. N. (2008). An Earth-system perspective of the global nitrogen cycle. *Nature Geoscience*, *451*, 293–296. https://doi.org/10.1038/nature06592

Heimann, M., Esser, G., Haxeltine, A., Kaduk, J., Kicklighter, D. W., Knorr, W., … Würth, G. (1998). Evaluation of terrestrial carbon cycle models through simulations of the seasonal cycle of atmospheric CO_2: First results of a model intercomparison study. *Global Biogeochemical Cycles*, *12*, 1–24. https://doi.org/10.1029/97gb01936

Hempel, S., Frieler, K., Warszawski, L., Schewe, J., & Piontek, F. (2013). A trend-preserving bias correction – The ISI-MIP approach. *Earth System Dynamics*, *4*, 219–236. https://doi.org/10.5194/esd-4-219-2013

Hiltbrunner, E., Körner, C., Meier, R., Braun, S., & Kahmen, A. (2019). Data do not support large-scale oligotrophication of terrestrial ecosystems. *Nature Ecology & Evolution*, *3*, 1285–1286. https://doi.org/10.1038/s41559-019-0948-5

Hofmockel, K. S., & Schlesinger, W. H. (2007). Carbon dioxide effects on heterotrophic dinitrogen fixation in a temperate pine forest. *Soil Science Society of America Journal*, *71*, 140–144. https://doi.org/10.2136/sssaj2006.110

Houlton, B. Z., Marklein, A. R., & Bai, E. (2015). Representation of nitrogen in climate change forecasts. *Nature Climate Change*, *5*, 398–401. https://doi.org/10.1038/nclimate2538

Hungate, B. A., Dukes, J. S., Shaw, M. R., Luo, Y., & Field, C. B. (2003). Nitrogen and climate change. *Science*, *302*, 1512–1513.

Hungate, B. A., Stiling, P. D., Dijkstra, P., Johnson, D. W., Ketterer, M. E., Hymus, G. J., … Drake, B. G. (2004). CO_2 elicits long-term decline in nitrogen fixation. *Science*, *304*, 1291. https://doi.org/10.1126/science.1095549

Hungate, B. A., van Groenigen, K. J., Six, J., Jastrow, J. D., Luo, Y., de Graff, M.-A., … Osenberg, C. W. (2009). Assessing the effect of elevated carbon dioxide on soil carbon: A comparison of four meta-analyses. *Global Change Biology*, *15*, 2020–2034. https://doi.org/10.1111/j.1365-2486.2009.01866.x

Huntzinger, D. N., Michalak, A. M., Schwalm, C., Ciais, P., King, A. W., & Fang, Y. (2017). Uncertainty in the response of terrestrial carbon sink to environmental drivers undermines carbon-climate feedback predictions. *Scientific Reports*, *7*, 4765. https://doi.org/10.1038/s41598-017-03818-2

Hurtt, G. C., Frolking, S., Fearon, M. G., Moore, B., Shevliakova, E., Malyshev, S., … Houghton, R. A. (2006). The underpinnings of land-use history: Three centuries of global gridded land-use transitions, wood-harvest activity, and resulting secondary lands. *Global Change Biology*, *12*, 1208–1229. https://doi.org/10.1111/j.1365-2486.2006.01150.x

Hyvönen, R., Agren, G. I., Linder, S., Persson, T., Cotrufo, M. F., Ekblad, A., … Wallin, G. (2007). The likely impact of elevated [CO_2], nitrogen deposition, increased temperature and management on carbon sequestration in temperate and boreal forest ecosystems: A literature review. *New Phytologist*, *173*, 463–480. https://doi.org/10.1111/j.1469-8137.2007.01967.x

Jacobson, A. R., Mikaloff Fletcher, S. E., Gruber, N., Sarmiento, J. L., & Gloor, M. (2007). A joint atmosphere-ocean inversion for surface

fluxes of carbon dioxide: 1. Methods and global-scale fluxes. *Global Biogeochemical Cycles*, *21*. https://doi.org/10.1029/2005GB002556

Jones, C., Robertson, E., Arora, V. K., Friedlingstein, P., Shevliakova, E., Bopp, L., … Tjiputra, J. (2013). 21st century compatible CO_2 emissions and airborne fraction simulated by CMIP5 Earth System models under 4 representative concentration pathways. *Journal of Climate*, *26*, 4398–4413. https://doi.org/10.1175-JCLI-D-12-00554.1

Jung, M., Reichstein, M., Margolis, H. A., Cescatti, A., Richardson, A. D., & Arain, M. A. (2011). Global patterns of land-atmosphere fluxes of carbon dioxide, latent heat, and sensible heat derived from eddy covariance, satellite, and meteorological observations. *Journal of Geophysical Research*, *116*, G00J07. https://doi.org/10.1029/2010jg001566

Kalnay, E., Kanamitsu, M., Kistler, R., Collins, W., Deaven, D., Gandin, L., … Joseph, D. (1996). The NCEP/NCAR 40-year reanalysis project. *Bulletin of the American Meteorological Society*, *77*, 437–472. https://doi.org/10.1175/1520-0477(1996)077<0437:TNYRP>2.0.CO;2

Kaminski, T., Heimann, M., & Giering, R. (1999). A coarse grid three-dimensional global inverse model of the atmospheric transport: 1. Adjoint model and Jacobian matrix. *Journal of Geophysical Research: Atmosphere*, *104*, 18535–18553. https://doi.org/10.1029/1999jd900147

Kattge, J., Daz, S., Lavorel, S., Prentice, I. C., Leadley, P., Boenisch, G., … Cornelissen, J. H. (2011). TRY – A global database of plant traits. *Global Change Biology*, *17*, 2905–2935.

Knyazikhin, Y., Schull, M. A., Stenberg, P., Mõttus, M., Rautiainen, M., Yang, Y., … Myneni, R. B. (2013). Hyperspectral remote sensing of foliar nitrogen content. *Proceedings of the National Academy of Sciences of the United States of America*, *110*, E185–E192. https://doi.org/10.1073/pnas.1210196109

Krinner, G., Viovy, N., de Noblet-Ducoudré, N., Ogée, J., Polcher, J., Friedlingstein, P., … Prentice, I. C. (2005). A dynamic global vegetation model for studies of the coupled atmosphere-biosphere system. *Global Biogeochemical Cycles*, *19*, GB1015. https://doi.org/10.1029/2003gb002199

Kull, O., & Kruijt, B. (1998). Leaf photosynthetic light response: A mechanistic model for scaling photosynthesis to leaves and canopies. *Functional Ecology*, *12*, 767–777. https://doi.org/10.1046/j.1365-2435.1998.00257.x

Lamarque, J.-F., Kyle, G. P., Meinshausen, M., Riahi, K., Smith, S. J., Vuuren, D. P., … Vitt, F. (2011). Global and regional evolution of short-lived radiatively-active gases and aerosols in the Representative Concentration Pathways. *Climatic Change*, *109*, 191–212. https://doi.org/10.1007/s10584-011-0155-0

Le Quéré, C., Andrew, R. M., Friedlingstein, P., Sitch, S. A., Pongratz, J., Manning, A. C., … Zhu, D. (2018). Global carbon budget 2017. *Earth System Science Data*, *10*, 405–448.

LeBauer, D. S., & Treseder, K. K. (2008). Nitrogen limitation of net primary productivity in terrestrial ecosystems is globally distributed. *Ecology*, *89*, 371–379. https://doi.org/10.1890/06-2057.1

Li, C. S., Aber, J., Stange, F., Butterbach-Bahl, K., & Papen, H. (2000). A process-oriented model of N_2O and NO emissions from forest soils: 1. Model development. *Journal of Geophysical Research-Atmospheres*, *105*, 4369–4384. https://doi.org/10.1029/1999jd900949

Liang, J., Qi, X., Souza, L., & Luo, Y. (2016). Processes regulating progressive nitrogen limitation under elevated carbon dioxide: A meta-analysis. *Biogeosciences*, *13*, 2689–2699. https://doi.org/10.5194/bg-13-2689-2016

Liu, Y. Y., van Dijk, A. I. J. M., McCabe, M. F., Evans, J. P., & de Jeu, R. A. M. (2013). Global vegetation biomass change (1988–2008) and attribution to environmental and human drivers. *Global Ecology and Biogeography*, *22*, 692–705. https://doi.org/10.1111/geb.12024

Magill, A. H., Aber, J. D., Currie, W. S., Nadelhoffer, K. J., Martin, M. E., McDowell, W. H., … Steudler, P. (2004). Ecosystem response to 15 years of chronic nitrogen additions at the Harvard Forest LTER, Massachusetts, USA. *Forest Ecology and Management*, *196*, 7–28. https://doi.org/10.1016/j.foreco.2004.03.033

Manzoni, S., Trofymow, J. A., Jackson, R., & Porporato, A. (2010). Stoichiometric controls on carbon, nitrogen, and phosphorus dynamics in decomposing litter. *Ecological Monographs*, *80*, 89–106. https://doi.org/10.1890/09-0179.1

McNulty, S. G., Boggs, J., Aber, J. D., Rustad, L., & Magill, A. (2005). Red spruce ecosystem level changes following 14 years of chronic N fertilization. *Forest Ecology and Management*, *219*, 279–291. https://doi.org/10.1016/j.foreco.2005.09.004

Medlyn, B. E., De Kauwe, M. G., Zaehle, S., Walker, A. P., Duursma, R. A., Luus, K., … Ellsworth, D. S. (2016). Using models to guide field experiments: A priori predictions for the CO_2 response of a nutrient- and water-limited native Eucalypt woodland. *Global Change Biology*, *22*, 2834–2851. https://doi.org/10.1111/gcb.13268

Medlyn, B. E., Zaehle, S., De Kauwe, M. G., Walker, A. P., Dietze, M. C., Hanson, P. J., … Norby, R. J. (2015). Using ecosystem experiments to improve vegetation models. *Nature Climate Change*, *5*, 528–534. https://doi.org/10.1038/nclimate2621

Meinshausen, M., Smith, S. J., Calvin, K., Daniel, J. S., Kainuma, M. L. T., Lamarque, J. F., … Vuuren, D. P. P. (2011). The RCP greenhouse gas concentrations and their extensions from 1765 to 2300. *Climatic Change*, *109*, 213–241. https://doi.org/10.1007/s10584-011-0156-z

Menge, D. N. L., Hedin, L. O., & Pacala, S. W. (2012). Nitrogen and phosphorus limitation over long-term ecosystem development in terrestrial ecosystems. *PLoS ONE*, *7*, 1–17.

Menge, D. N. L., Levin, S. A., & Hedin, L. O. (2008). Evolutionary tradeoffs can select against nitrogen fixation and thereby maintain nitrogen limitation. *Proceedings of the National Academy of Sciences of the United States of America*, *105*, 1573–1578. https://doi.org/10.1073/pnas.0711411105

Meyerholt, J., Sickel, K., & Zaehle, S. (2019). *O-CN ensemble version, rev 295*. Retrieved from https://projects.bgc-jena.mpg.de/OCN/browser/branches/bnfdev

Meyerholt, J., & Zaehle, S. (2015). The role of stoichiometric flexibility in modelling forest ecosystem responses to nitrogen fertilization. *New Phytologist*, *208*, 1042–1055. https://doi.org/10.1111/nph.13547

Meyerholt, J., & Zaehle, S. (2018). Controls of terrestrial ecosystem nitrogen loss on simulated productivity responses to elevated CO_2. *Biogeosciences*, *15*, 5677–5698. https://doi.org/10.5194/bg-15-5677-2018

Meyerholt, J., Zaehle, S., & Smith, M. J. (2016). Variability of projected terrestrial biosphere responses to elevated levels of atmospheric CO_2 due to uncertainty in biological nitrogen fixation. *Biogeosciences*, *13*, 1491–1518. https://doi.org/10.5194/bg-13-1491-2016

Mikaloff Fletcher, S. E., Gruber, N., Jacobson, A. R., Gloor, M., Doney, S. C., Dutkiewicz, S., … Sarmiento, J. L. (2006). Inverse estimates of anthropogenic CO_2 uptake, transport, and storage by the ocean. *Global Biogeochemical Cycles*, *20*. https://doi.org/10.1029/2005GB002530

Mikaloff Fletcher, S. E., Gruber, N., Jacobson, A. R., Gloor, M., Doney, S. C., Dutkiewicz, S., … Sarmiento, J. L. (2007). Inverse estimates of the oceanic sources and sinks of natural CO_2 and the implied oceanic carbon transport. *Global Biogeochemical Cycles*, *21*. https://doi.org/10.1029/2006GB002751

Norby, R. J., De Kauwe, M. G., Domingues, T. F., Duursma, R. A., Ellsworth, D. S., Goll, D. S., … Zaehle, S. (2016). Model–data synthesis for the next generation of forest free-air CO_2 enrichment (FACE) experiments. *New Phytologist*, *209*, 17–28. https://doi.org/10.1111/nph.13593

Norby, R. J., De Kauwe, M. G., Walker, A. P., Werner, C., Zaehle, S., & Zak, D. R. (2017). Comment on "Mycorrhizal association as a primary control of the CO_2 fertilization effect". *Science*, *355*, 358. https://doi.org/10.1126/science.aai7976

Ollinger, S. V., Richardson, A. D., Martin, M. E., Hollinger, D. Y., Frolking, S. E., Reich, P. B., … Schmid, H. P. (2008). Canopy nitrogen,

carbon assimilation, and albedo in temperate and boreal forests. *Proceedings of the National Academy of Sciences of the United States of America*, *105*, 19336–19341. https://doi.org/10.1073/pnas.0810021105

Rastetter, E. B., Vitousek, P. M., Field, C., Shaver, G. R., Herbert, D., & gren, G. I. (2001). Resource optimization and symbiotic nitrogen fixation. *Ecosystems*, *4*, 369–388. https://doi.org/10.1007/s10021-001-0018-z

Righi, M., Andela, B., Eyring, V., Lauer, A., Predoi, V., Schlund, M., … Zimmermann, K. (2019). ESMValTool v2.0 – Technical overview. *Geoscientific Model Development Discussions*. https://doi.org/10.5194/gmd-2019-226

Rödenbeck, C., Houweling, S., Gloor, M., & Heimann, M. (2003). CO_2 flux history 1982–2001 inferred from atmospheric data using a global inversion of atmospheric transport. *Atmospheric Chemistry and Physics*, *3*, 1919–1964. https://doi.org/10.5194/acp-3-1919-2003

Saugier, B., & Roy, J. (2001). Estimations of global terrestrial productivity: Converging towards a single number? In H. Mooney, J. Roy, & B. Saugier (Eds.), *Global terrestrial productivity: Past, present and future*. San Diego, CA: Academic Press.

Schulte-Uebbing, L., & de Vries, W. (2018). Global-scale impacts of nitrogen deposition on tree carbon sequestration in tropical, temperate, and boreal forests: A meta-analysis. *Global Change Biology*, *24*, e416–e431. https://doi.org/10.1111/gcb.13862

Smith, B., Wårlind, D., Arneth, A., Hickler, T., Leadley, P., Siltberg, J., & Zaehle, S. (2014). Implications of incorporating N cycling and N limitations on primary production in an individual-based dynamic vegetation model. *Biogeosciences*, *11*, 2027–2054. https://doi.org/10.5194/bg-11-2027-2014

Sokolov, A. P., Kicklighter, D. W., Melillo, J. M., Felzer, B. S., Schlosser, C. A., & Cronin, T. W. (2008). Consequences of considering carbon-nitrogen interactions on the feedbacks between climate and the terrestrial carbon cycle. *Journal of Climate*, *21*, 3776–3796. https://doi.org/10.1175/2008JCLI2038.1

Sulman, B. N., Shevliakova, E., Brzostek, E. R., Kivlin, S. N., Malyshev, S., Menge, D. N., & Zhang, X. (2019). Diverse mycorrhizal associations enhance terrestrial C storage in a global model. *Global Biogeochemical Cycles*, *33*, 501–523. https://doi.org/10.1029/2018GB005973

Terrer, C., Vicca, S., Hungate, B. A., Phillips, R. P., & Prentice, I. C. (2016). Mycorrhizal association as a primary control of the CO_2 fertilization effect. *Science*, *353*, 72–74. https://doi.org/10.1126/science.aaf4610

Thomas, R. Q., Brookshire, E. N. J., & Gerber, S. (2015). Nitrogen limitation on land: How can it occur in Earth system models? *Global Change Biology*, *21*, 1777–1793. https://doi.org/10.1111/gcb.12813

Thomas, R. Q., Zaehle, S., Templer, P. H., & Goodale, C. L. (2013). Global patterns of nitrogen limitation: Confronting two global biogeochemical models with observations. *Global Change Biology*, *19*, 2986–2998. https://doi.org/10.1111/gcb.12281

Thornton, P. E., Doney, S. C., Lindsay, K., Moore, J. K., Mahowald, N., Randerson, J. T., … Lee, Y.-H. (2009). Carbon-nitrogen interactions regulate climate-carbon cycle feedbacks. *Biogeosciences*, *6*, 2099–2120. https://doi.org/10.5194/bg-6-2099-2009

Thornton, P. E., Lamarque, J. F., Rosenbloom, N. A., & Mahowald, N. M. (2007). Influence of carbon-nitrogen cycle coupling on land model response to CO_2 fertilization and climate variability. *Global Biogeochemical Cycles*, *21*. https://doi.org/10.1029/2006GB002868

Thornton, P. E., & Rosenbloom, N. A. (2005). Ecosystem model spin-up: Estimating steady state conditions in a coupled terrestrial carbon and nitrogen cycle model. *Ecological Modelling*, *189*, 25–48. https://doi.org/10.1016/j.ecolmodel.2005.04.008

Tian, H., Yang, J., Xu, R., Lu, C., Canadell, J. G., Davidson, E. A., … Zhang, B. (2019). Global soil nitrous oxide emissions since the preindustrial era estimated by an ensemble of terrestrial biosphere models: Magnitude, attribution, and uncertainty. *Global Change Biology*, *25*, 640–659. https://doi.org/10.1111/gcb.14514

Townsend, P. A., Serbin, S. P., Kruger, E. L., & Gamon, J. A. (2013). Disentangling the contribution of biological and physical properties of leaves and canopies in imaging spectroscopy data. *Proceedings of the National Academy of Sciences of the United States of America*, *110*(12), E1074. https://doi.org/10.1073/pnas.1300952110

Vicca, S., Stocker, B. D., Reed, S., Wieder, W. R., Bahn, M., Fay, P. A., … Ciais, P. (2018). Using research networks to create the comprehensive datasets needed to assess nutrient availability as a key determinant of terrestrial carbon cycling. *Environmental Research Letters*, *13*, 125006–125014. https://doi.org/10.1088/1748-9326/aaeae7

Viovy, N. (2016). *CRUNCEP data set*. Retrieved from ftp://nacp.ornl.gov/synthesis/2009/frescati/temp/land_use_change/original/readme.htm

Vitousek, P. M., Cassman, K., Cleveland, C., Crews, T., Field, C. B., Grimm, N. B., … Sprent, J. I. (2002). Towards an ecological understanding of biological nitrogen fixation. *Biogeochemistry*, *57*(58), 1–45.

Vitousek, P. M., & Howarth, R. W. (1991). Nitrogen limitation on land and in the sea – How it can occur. *Biogeochemistry*, *13*, 87–115.

Vitousek, P. M., Menge, D. N. L., Reed, S. C., & Cleveland, C. C. (2013). Biological nitrogen fixation: Rates, patterns and ecological controls in terrestrial ecosystems. *Philosophical Transactions of the Royal Society B: Biological Sciences*, *368*, 20130119. https://doi.org/10.1098/rstb.2013.0119

Walker, A. P., Zaehle, S., Medlyn, B. E., De Kauwe, M. G., Asao, S., Hickler, T., … Norby, R. J. (2015). Predicting long-term carbon sequestration in response to CO_2 enrichment: How and why do current ecosystem models differ? *Global Biogeochemical Cycles*, *29*, 476–495. https://doi.org/10.1002/2014gb004995

Wang, Y. P., Law, R. M., & Pak, B. (2010). A global model of carbon, nitrogen and phosphorus cycles for the terrestrial biosphere. *Biogeosciences*, *7*, 2261–2282. https://doi.org/10.5194/bg-7-2261-2010

Wårlind, D., Smith, B., Hickler, T., & Arneth, A. (2014). Nitrogen feedbacks increase future terrestrial ecosystem carbon uptake in an individual-based dynamic vegetation model. *Biogeosciences*, *11*, 6131–6146. https://doi.org/10.5194/bg-11-6131-2014

Wieder, W. R., Cleveland, C. C., Lawrence, D. M., & Bonan, G. B. (2015). Effects of model structural uncertainty on carbon cycle projections: Biological nitrogen fixation as a case study. *Environmental Research Letters*, *10*(4), 044016. https://doi.org/10.1088/1748-9326/10/4/044016

Wieder, W. R., Cleveland, C. C., Smith, W. K., & Todd-Brown, K. (2015). Future productivity and carbon storage limited by terrestrial nutrient availability. *Nature Geoscience*, *8*, 441–444. https://doi.org/10.1038/ngeo2413

Xu-Ri, & Prentice, I. C. (2008). Terrestrial nitrogen cycle simulation with a dynamic global vegetation model. *Global Change Biology*, *14*, 1745–1764. https://doi.org/10.1111/j.1365-2486.2008.01625.x

Xu-Ri, & Prentice, I. C. (2017). Modelling the demand for new nitrogen fixation by terrestrial ecosystems. *Biogeosciences*, *14*, 2003–2017. https://doi.org/10.5194/bg-14-2003-2017

Yang, X., Wittig, V., Jain, A. K., & Post, W. (2009). The integration of nitrogen cycle dynamics into the Integrated Science Assessment Model (ISAM) for the study of terrestrial ecosystem responses to global change. *Global Biogeochemical Cycles*, *23*, GB4029. https://doi.org/10.1029/2009GB003474

Zaehle, S., Ciais, P., Friend, A. D., & Prieur, V. (2011). Carbon benefits of anthropogenic reactive nitrogen offset by nitrous oxide emissions. *Nature Geoscience*, *4*, 601–605. https://doi.org/10.1038/ngeo1207

Zaehle, S., & Dalmonech, D. (2011). Carbon–nitrogen interactions on land at global scales: Current understanding in modelling climate biosphere feedbacks. *Current Opinion in Environmental*

Sustainability, *3*, 311–320. https://doi.org/10.1016/j.cosust.2011.08.008

Zaehle, S., Friedlingstein, P., & Friend, A. D. (2010). Terrestrial nitrogen feedbacks may accelerate future climate change. *Geophysical Research Letters*, *37*, L01401. https://doi.org/10.1029/2009gl041345

Zaehle, S., & Friend, A. D. (2010). Carbon and nitrogen cycle dynamics in the O-CN land surface model: 1. Model description, site-scale evaluation, and sensitivity to parameter estimates. *Global Biogeochemical Cycles*, *24*. https://doi.org/10.1029/2009gb003521

Zaehle, S., Friend, A. D., Friedlingstein, P., Dentener, F., Peylin, P., & Schulz, M. (2010). Carbon and nitrogen cycle dynamics in the O-CN land surface model: 2. Role of the nitrogen cycle in the historical terrestrial carbon balance. *Global Biogeochemical Cycles*, *24*(1). https://doi.org/10.1029/2009GB003522

Zaehle, S., Jones, C. D., Houlton, B. Z., Lamarque, J.-F., & Robertson, E. (2015). Nitrogen availability reduces CMIP5 projections of 21st century land carbon uptake. *Journal of Climate*, *28*, 2494–2511. https://doi.org/10.1175/jcli-d-13-00776.1

Zaehle, S., Medlyn, B. E., De Kauwe, M. G., Walker, A. P., Dietze, M. C., Hickler, T., … Norby, R. J. (2014). Evaluation of 11 terrestrial carbon-nitrogen cycle models against observations from two temperate Free-Air CO_2 Enrichment studies. *New Phytologist*, *202*, 803–822. https://doi.org/10.1111/nph.12697

Zhang, Q., Wang, Y.-P., Matear, R., Pitman, A. J., & Dai, Y. J. (2014). Nitrogen and phosphorus limitations significantly reduce future allowable CO_2 emissions. *Geophysical Research Letters*, *41*, 632–637. https://doi.org/10.1002/2013gl058352

Zheng, M., Zhou, Z., Luo, Y., Zhao, P., & Mo, J. (2019). Global pattern and controls of biological nitrogen fixation under nutrient enrichment: A meta-analysis. *Global Change Biology*, *25*, 3018–3030. https://doi.org/10.1111/gcb.14705

SUPPORTING INFORMATION

Additional supporting information may be found online in the Supporting Information section.

How to cite this article: Meyerholt J, Sickel K, Zaehle S. Ensemble projections elucidate effects of uncertainty in terrestrial nitrogen limitation on future carbon uptake. *Glob Change Biol*. 2020;26:3978–3996. https://doi.org/10.1111/gcb.15114